Aus dem Institut für Pathologie
der Universität zu Köln
Direktor: Universitätsprofessor Dr. med. R. Büttner

Clonal evolution and resistance mechanisms in *BRAF*-driven *EGFR*-mutated lung cancer

Inaugural-Dissertation zur Erlangung der Doktorwürde
der Medizinischen Fakultät
der Universität zu Köln

vorgelegt von
David Fabian Ast
aus Bergisch Gladbach

promoviert am 18. Dezember 2025

Gedruckt mit Genehmigung der Medizinischen Fakultät der Universität zu Köln

Druckjahr 2026

Dekan:	Universitätsprofessor Dr. med. G. R. Fink
1. Gutachter:	Professor Dr. med. M. Sos
2. Gutachter:	Privatdozent Dr. med. M. Scheffler

Erklärung

Ich erkläre hiermit, dass ich die vorliegende Dissertationsschrift ohne unzulässige Hilfe Dritter und ohne Benutzung anderer als der angegebenen Hilfsmittel angefertigt habe; die aus fremden Quellen direkt oder indirekt übernommenen Gedanken sind als solche kenntlich gemacht.

Bei der Auswahl und Auswertung des Materials sowie bei der Herstellung des Manuskriptes habe ich keine Unterstützungsleistungen erhalten.

Weitere Personen waren an der Erstellung der vorliegenden Arbeit nicht beteiligt. Insbesondere habe ich nicht die Hilfe einer Promotionsberaterin/eines Promotionsberaters in Anspruch genommen. Dritte haben von mir weder unmittelbar noch mittelbar geldwerte Leistungen für Arbeiten erhalten, die im Zusammenhang mit dem Inhalt der vorgelegten Dissertationsschrift stehen.

Die Dissertationsschrift wurde von mir bisher weder im Inland noch im Ausland in gleicher oder ähnlicher Form einer anderen Prüfungsbehörde vorgelegt.

Die in dieser Arbeit bzw. dem Paper ab der Überschrift „Resistance through the selection of $BRAF^{V600E}$-positive clones angegebenen Daten, Ergebnisse und Experimente (Figure 2 und 3; Supplemental Figure 5-13) wurden von mir oder unter meiner Mitarbeit gesammelt bzw. durchgeführt. Bei der Sammlung und Bearbeitung der klinischen (Patienten-)Daten (Figure 1; Supplemental Figure 1-4) sowie Betreuung der Patienten war ich nicht beteiligt.

Die in dieser Arbeit angegebenen Experimente sind nach entsprechender Anleitung durch Herrn Martin Sos und Herrn Johannes Brägelmann von mir selbst ausgeführt worden. Darunter fallen folgende Laborschritte bzw. Experimente:
Zellkultur, Klonierung und Einbringung der viralen Vektoren zur Überexpression von $BRAF^{V600E}$ und $NRAS^{Q61K}$ in die Zelllinien, Generierung resistenter Zelllinien, Crystal violet-Assay, Western Blot, PCR, RTqPCR, Gel-Elektrophorese, CTG-Assay, Synergy Screen, Wachstumsreihen, Klonalitäts-Assay, Generierung und Vorbereitung der Zellen für die in vivo Experimente.

Die Durchflusszytometrische Bestimmung der Apoptoserate wurde von Frau Hannah Tumbrink (Supplemental Figure 6a und 8) durchgeführt.

Die in vivo Experimente wurden von Frau Hannah Tumbrink unter Mithilfe von Frau Inga Spille und Frau Steffanie Lennartz durchgeführt.

Die in dieser Arbeit entstandenen Messwerte sind nach entsprechender Anleitung durch Herrn Martin Sos und Herrn Johannes Brägelmann von mir selbst ausgewertet worden. Dafür wurde die Statistiksoftware „R“ oder Mikrosoft Excel benutzt. Dies bezieht sich auf alle oben genannten von mir durchgeführten Experimente sowie die in vivo Daten.

Die Auswertung der RNA-Sequenzierung (Figure 2 E; Supplementary Figure 6D und 7A) fand durch Herrn Johannes Brägelmann statt.

Erklärung zur guten wissenschaftlichen Praxis:

Ich erkläre hiermit, dass ich die Ordnung zur Sicherung guter wissenschaftlicher Praxis und zum Umgang mit wissenschaftlichem Fehlverhalten (Amtliche Mitteilung der Universität zu Köln AM 132/2020) der Universität zu Köln gelesen habe und verpflichte mich hiermit, die dort genannten Vorgaben bei allen wissenschaftlichen Tätigkeiten zu beachten und umzusetzen.

David Fabian Ast
Köln, den 21.01.2026

Danksagung

An dieser Stelle möchte ich allen danken, die mich bei der Anfertigung meiner Doktorarbeit unterstützt haben.

Mein besonderer Dank gilt Martin und Johannes für die hervorragende Betreuung und Unterstützung, ohne die diese Arbeit so sicher nicht entstanden wäre.

Außerdem möchte ich mich insbesondere bei Marcel und Hannah für die schnelle und kompetente Durchsicht dieser Arbeit und die zahlreichen Verbesserungsvorschläge bedanken.

In den Jahren im Labor habe ich unzählige tolle Menschen kennengelernt, von denen ich viele mittlerweile zu meinen engsten Freunden zählen darf. Ich danke euch für die fachliche und emotionale Unterstützung – bei egal wie blöden Fragen und Problemen, zu jeder denkbaren Zeit. Ich bin dankbar für die unvergesslichen Feiern und „Beer Hours“. Danke, Marcel, Hannah, Carina, Laura, Mareike, Katharina, Lisa – um nur einige zu nennen.

Für die finanzielle Unterstützung dieser Arbeit danke ich der Mildred Scheel School of Oncology für das Forschungsstipendium, Martin für die zeitweise Anstellung als studentische Hilfskraft und meiner Familie für die Unterstützung, ohne die ich meine Zeit nicht so zielgerichtet auf dieses Projekt hätte fokussieren können.

Meinen Eltern, meiner Familie, meinen Freunden und nicht zuletzt meiner Freundin danke ich für ihre Ermutigungen, Zusprüche und ihren Glauben an mich – in Momenten, in denen ich selbst gezweifelt habe.

Ich widme diese Arbeit meinen Eltern, Ina und Falk, sowie meinen Omas, Gudrun und Helga.
Ihr habt all die Jahre an mich geglaubt und mich bei allem unterstützt.
Ich bin froh, euch zu haben.

Table of contents

List of abbreviations

ATP	adenosine triphosphate
BRAF	v-Raf murine sarcoma viral oncogene homolog B1
EGF	epidermal growth factor
EGFR	epidermal growth factor receptor
ErbB	erythroblastic leukaemia viral oncogene homolog B
ERK	extracellular-signal regulated kinase
EGR	early growths response protein
FDA	U.S. Food and Drug Administration
GDP	guanosine diphosphate
Grb2	growth factor receptor-bound protein 2
GTP	guanosine triphosphate
HRAS	Harvey rat sarcoma viral oncogene homolog
HER2	human epidermal growth factor receptor 2
KRAS	Kirsten rat sarcoma viral oncogene homolog
KSR	kinase suppressor of RAS
LUAD	lung adenocarcinoma
MAPK	mitogen-activated protein kinase
MEK	mitogen-activated protein kinase kinase
MET	mesenchymal epithelial transition factor
mRNA	messenger RNA
NRAS	neuroblastoma RAS viral oncogene homolog
NSCLC	non-small cell lung cancer
RAF	rapidly accelerated fibrosarcoma kinase
RAS	rat sarcoma viral oncogene homolog
RET	rearranged during transfection
RTK	receptor tyrosine kinase
SCLC	small cell lung cancer
SOS	son of sevenless
TKI	tyrosine kinase inhibitor
WES	whole exome sequencing

1. Zusammenfassung

Trotz des klinischen Erfolges der Drittgenerations-Tyrosinkinase-Inhibitoren (TKI) des epidermalen Wachstumsfaktorrezeptors (EGFR) stellt die TKI-Therapie erworbene Resistenz nach wie vor eine bedeutende Einschränkung bei der Behandlung von nicht-kleinzelligem Lungenkrebs (NSCLC) dar. In dieser Studie wird eine Kohorte von Patienten mit gleichzeitig auftretenden *EGFR*- und *BRAF*-Mutationen sowohl bei der Erstdiagnose als auch als Resistenzmechanismus nach einer EGFR-TKI-Therapie untersucht. Mithilfe von Whole-Exom-Sequenzierung (WES) multipler Biopsien einzelner Patienten konnten die klonale Entwicklung der entdeckten Subklone und ihre jeweiligen Resistenz- und Entstehungsmechanismen beschrieben werden.

Die Ergebnisse mehrerer Studien haben gezeigt, dass Zellen mit gleichzeitigen *EGFR*- und *KRAS*-Mutationen eine synthetische Letalität aufweisen[1–3]. In dieser Arbeit wurde untersucht, ob die gleichzeitige Überexpression von EGFR und BRAF zu einer ähnlichen zytotoxischen Wirkung führen. Funktionelle Untersuchungen ergaben, dass NSCLC-Zelllinien aus Patienten mit einer Koexpression von $EGFR^{del19}$ und $BRAF^{V600E}$-Mutationen durch eine anhaltende Aktivierung des MAPK-Signalwegs eine Resistenz gegen eine EGFR-TKI-Therapie aufweisen. Es wurden jedoch keine Fitnessnachteile oder synthetische Letalität beobachtet.

Die Ergebnisse zeigen, dass die $BRAF^{V600E}$-Mutation bei *EGFR*-mutiertem NSCLC ein robuster und relevanter Resistenzmechanismus gegen eine EGFR-TKI-Therapie ist. Die Studie zeigt die klinische Relevanz von *BRAF*-Mutationen in NSCLC-Patienten und das Potenzial, MAPK-Signalweg vermittelte Resistenzen durch die kombinierte, vertikale Inhibition von EGFR und MEK1/2 zu überwinden. Diese Kombinationstherapie mittels osimertinib und trametinib unterdrückte das Tumorwachstum *in vitro* sowie *in vivo* in murinen Xenograft-Modellen.

1.1 Summary

Despite the clinical success of third-generation epidermal growth factor receptor (EGFR) tyrosine kinase inhibitors (TKIs), acquired resistance remains a key limitation for the treatment of non-small cell lung cancer (NSCLC). This study investigates co-occurring *EGFR* and *BRAF* mutations at initial diagnosis and as resistance mechanism after EGFR-TKI therapy in a cohort of patients. Using whole-exome sequencing (WES) of multiple biopsies from individual patients provided insights into the clonal evolution of detected subclones and their respective mechanisms of resistance as well as their origin.

The findings of multiple studies have shown that cells with co-occurring *EGFR* and *KRAS* mutations exhibit synthetic lethality[1–3]. This work explored whether simultaneous overexpression of EGFR and BRAF could result in a similar synthetic lethal cytotoxic effect. Our functional studies revealed that patient-derived NSCLC cells harbouring co-expression of $EGFR^{del19}$ and $BRAF^{V600E}$ mutations are resistant to EGFR-TKI therapy through sustained activation of the MAPK signalling pathway. However, no fitness disadvantages or synthetic lethality were observed.

The study demonstrated that $BRAF^{V600E}$ in EGFR-mutant NSCLC is a robust and relevant mechanism of resistance against EGFR TKI therapy. The study also highlighted the clinical relevance of *BRAF* mutations in NSCLC patients and the potential to overcome MAPK pathway-mediated resistance through combined vertical inhibition of EGFR and MEK1/2. This combination therapy of osimertinib and trametinib suppressed tumour growth *in vitro* and in *in vivo* mouse xenograft models.

2. Introduction

2.1. Lung cancer

Lung cancer is the leading cause of cancer-related deaths worldwide, with an incidence of almost 2.5 million new cases and about 1.8 million deaths per year[4]. Lung cancer can be divided histologically into small cell lung cancer (SCLC) and non-small cell lung cancer (NSCLC), with NSCLC accounting for about 85 % of cases (**Figure 1**)[5]. The majority of NSCLC patients present with lung adenocarcinomas (LUAD) that originate from alveolar type II (ATII) cells while the rest primarily show squamous differentiations. The primary risk factor for lung cancer is tobacco smoking, which is responsible for 80-90 % of all cases. Less prevalent are other risk factors such as passive smoking, radiation, asbestos, and pre-existing lung diseases[6].

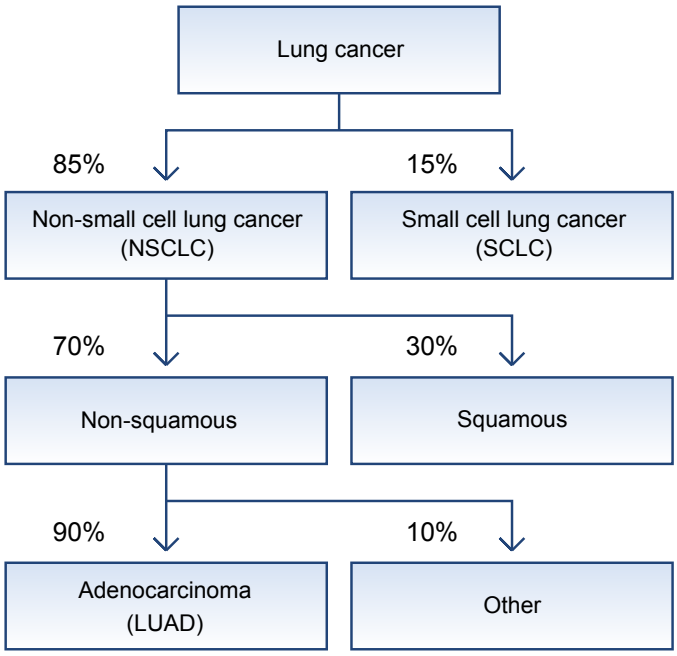

Figure 1. Schematic overview of lung cancer classification with frequency distribution. 15 % of lung cancers are classified as small cell lung cancer (SCLC), with the remaining 85 % classified as non-small cell lung cancer (NSCLC). NSCLC can be divided into squamous (30 %) and non-squamous (70 %). Of the latter, the majority (90 %) are adenocarcinomas, which can also be further subdivided histologically. (adapted from Gridelli et al., 2015)[5]

2.2 Carcinogenesis of lung adenocarcinoma

LUAD develops through the acquisition of genetic mutations, deletions, translocations, or amplifications (**Figure 2**). Some of the most frequently occurring mutations in NSCLC are those

affecting the genes of the epidermal growth factor receptor (*EGFR*), with a prevalence of 10-35 %, the Kirsten-Rat Sarcoma virus (*KRAS*), with a prevalence of 15-25 %, the v-Raf murine sarcoma viral oncogene homolog B1 (*BRAF*), with a prevalence of 1-3 % and Neuroblastoma RAS viral oncogene homolog (*NRAS*) with a prevalence of 1 % of NSCLC cases[6]. The proteins encoded by these genes all function within the mitogen-activated protein kinase (MAPK) pathway[7], which triggers cell growth and proliferation upon stimulation by mitogens.

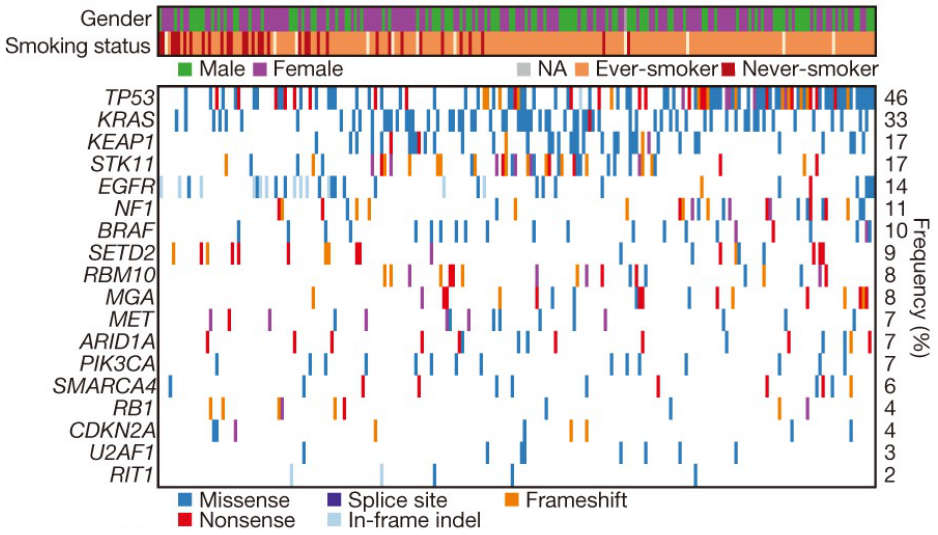

Figure 2. Genetic landscape in LUAD. Co-mutation plot from whole exome sequencing of 230 lung adenocarcinomas. The upper bar displays the gender and smoking status of the individuals. The lower part of the graph shows the significantly altered genes (corrected P value less than 0.025) in order of prevalence. The colour coding is used to specify the type of genetic alteration. (Modified from EA Collisson et al./ The Cancer Genome Atlas Research Network, 2014)[8]

2.3 MAPK-pathway

The MAPK pathway is a crucial signalling cascade that transmits signals from extracellular mitogens like the epidermal growth factor (EGF) to the nucleus, leading to gene expression changes that promote cell growth, proliferation, and differentiation. Signalling is initiated when the ligand (e.g. EGF) binds to its receptor, (e.g. EGFR, a receptor tyrosine kinase (RTK)) located on the cell membrane. This binding induces homo- or hetero-dimerization of EGFR, leading to phosphorylation of tyrosine residues in the *C*-terminal tail. The phosphorylated tyrosine residues on EGFR serve as docking sites for adaptor proteins such as growth factor receptor-bound protein 2 (Grb2), which recruits Son of Sevenless (SOS), a guanine nucleotide exchange factor. SOS activates RAS, a small GTPase, by facilitating the exchange of GDP for GTP on RAS. Once activated, RAS activates RAF, a serine/threonine kinase. This activation involves the binding of RAF to GTP-bound RAS at the plasma membrane, leading to the activation and subsequent phosphorylation of RAF. The process of signal transduction from RAF to ERK is facilitated by the formation of a RAF-MEK-ERK complex, which is enabled by

kinase suppressor of RAS (KSR) proteins. Activated RAF phosphorylates and activates MAPK/ERK kinase 1/2 (MEK1/2), a dual-specificity kinase that can phosphorylate both serine/threonine and tyrosine residues. MEK1/2 phosphorylates extracellular-signal-regulated kinase 1/2 (ERK 1/2) on both threonine and tyrosine residues, leading to its activation. Once activated, ERK1/2 translocates to the nucleus, where it phosphorylates various families of transcription factors such as MYC, EGR and FOS. This ultimately leads to changes in gene expression that drive cell growth, proliferation and differentiation (**Figure 3**)[7,9–12].

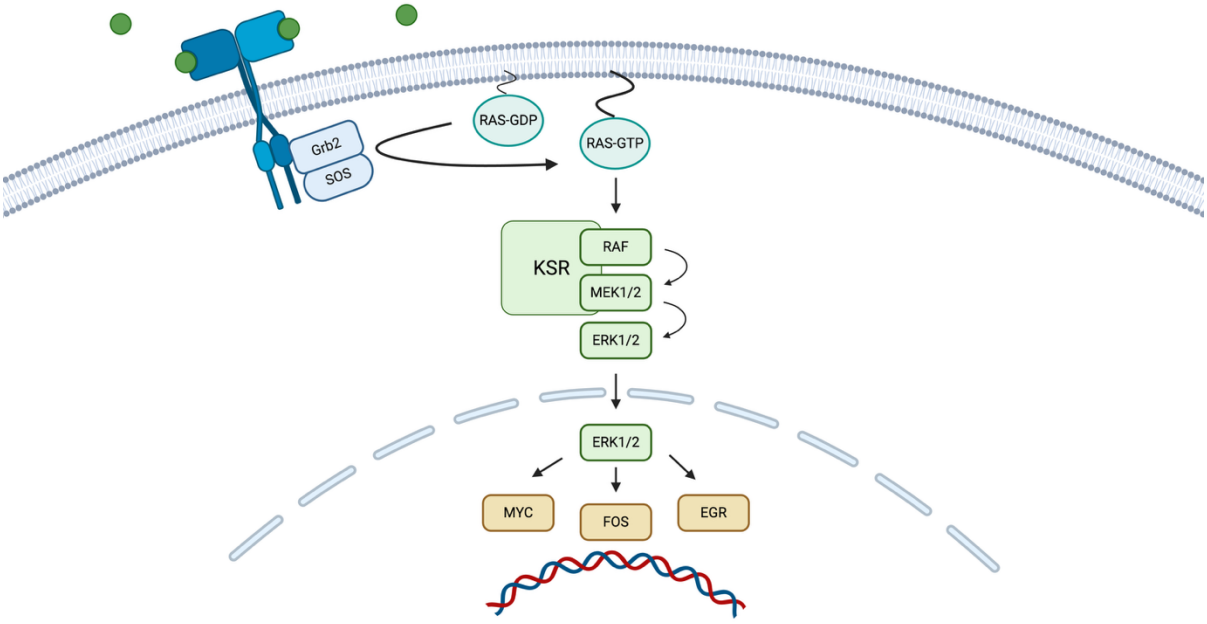

Figure 3. Simplified schematic representation of the RAS/RAF/MEK/ERK MAPK pathway initiated via EGF-binding. The binding of EGF to EGFR results in the activation of RAS, which is facilitated by Grb2 and SOS. RAS, in turn, activates the mitogen-activated protein kinase (MAPK) pathway, initiating a signalling cascade via RAF, MEK and ERK facilitated by KSR. Activated ERK translocates into the nucleus, where it phosphorylates different families of transcription factors, ultimately resulting in cell growth and differentiation. (modified from Ullah et al., 2021)[12]

2.3.1. EGFR

The ErbB protein family consists of four RTKs: ErbB 1 (EGFR), ErbB 2 (HER2), ErbB 3 and ErbB 4. EGFR and HER2 can often be found as oncogenes in many different cancer entities[13]. The most common therapeutically tractable driver mutations observed in LUAD are those that result in activation of the EGFR gene. These mutations display ethnic-specific differences in frequency, with higher prevalence in Asians (40–60 %) compared to Caucasians (7–10 %)[14]. The most prevalent EGFR alterations observed in NSCLC are deletion-mutations in exon 19 (45 %) and the point-mutation *EGFR*^{L858R} (40-45 %), which occurs in the activation loop region of exon 21 (**Figure 4**)[15]. Some mutations are predominantly identified in relapsed tumours as a resistance mechanism against targeted therapy, exemplified by *EGFR*^{T790M} and *EGFR*^{C797S}

[16]. Activating mutations within the kinase domain result in the constitutive activation of EGFR leading to aberrant signalling via the MAPK-pathway among others[17].

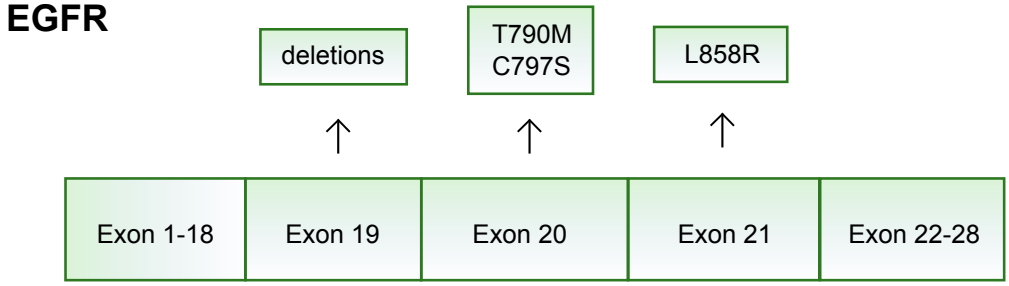

Figure 4. *EGFR* mutations. Schematic representation of the most common EGFR mutations with reference to the affected exon. (adapted from O´Leary et al. 2020)[17]

2.3.2. RAS

RAS is one of the most frequently mutated oncogenes, with a prevalence of approximately 15-19 % across all cancer subtypes[18]. The prevalence varies between the three isoforms, with KRAS being responsible for about 75 % of the cases, followed by NRAS with about 17 % and Harvey rat sarcoma virus (HRAS) with about 7 %[18,19]. While KRAS alterations are most common in pancreatic, colorectal and LUAD cancers, NRAS alterations are most prevalent in skin, thyroid and haematopoietic cancers[18–20]. The most frequent mutations in *RAS* are activating mutations in codon 12, 13 or 61, which lead to reduced intrinsic GTPase activity, resulting in a prolonged half-life of GTP-loaded RAS whereby it becomes constitutively active [9,11,19]. Five mutations (*G12D*, *G12V*, *G12C*, *G13D* and *Q61R*) account for 70 % of all *RAS* mutant patients (**Figure 5**)[19]. Due to transversions associated with bulky adducts produced by mutagens in tobacco smoke, *G12C* mutations are often found in lung cancer[19].

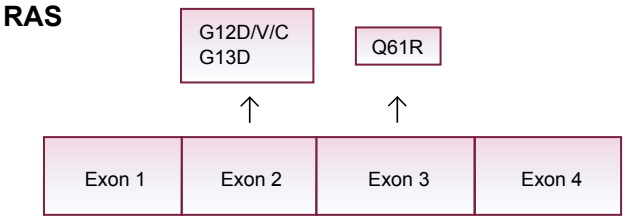

Figure 5. *RAS* mutations. Schematic representation of the most common *RAS* mutations with reference to the affected exon. (adapted from Prior, Hood and Hartley, 2020)[19]

2.3.3. BRAF

BRAF, along with ARAF and CRAF (also known as RAF1), is a member of the rapid accelerated fibrosarcoma (RAF) kinase family[9,11,21]. Mutations in the *BRAF* gene are found in about 7-8 % of all cancers[20–23]. They are frequently found in malignant melanoma (about 66%) and are also commonly found in colorectal cancer, thyroid cancer and NSCLC, with *BRAF*^{V600E} being by far the most frequent[20,22,23]. *BRAF* mutations can be divided into 3 classes[24,25]. Class 1 are *BRAF* mutations in codon 600 (*V600E/K/D/R/M*). These mutations result in RAS-independent signalling as activated monomers. Class 2 mutations are defined as non-V600 mutations that result in RAS-independent signalling as activated dimers[24,25]. These include mutations in codons 464 (*G464V/E*), 469 (*G469A/V/R*), 597 (*L597Q/V*) and 601 (*K601E/N/T*) (**Figure 6**). While class 1 and 2 mutations result in increased kinase activity compared to wild-type BRAF, class 3 mutations are known as "kinase-dead" with no or reduced kinase activity[24,25]. They are unable to activate MEK1/2 but are able to bind to CRAF in a RAS-dependent manner to transduce signals[24–26]. Therefore, class 3 mutations are often found in combination with RAS alterations[24,26].

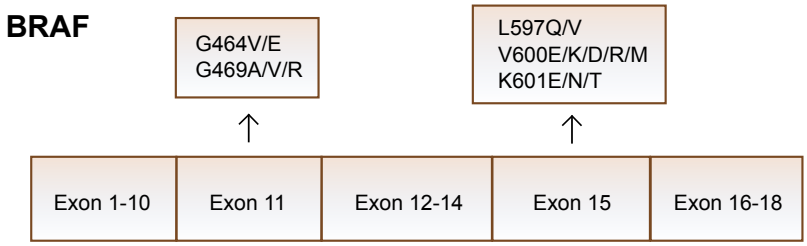

Figure 6. *BRAF* mutations. Schematic representation of the most common BRAF mutations with reference to the affected exon. (adapted from Yao et al. 2017)[24]

2.4 Targeted therapy

The treatment of NSCLC is complex and involves a multimodal interplay between different approaches and medical specialties. The most definitive and, if possible, preferred therapy is complete surgical removal of the tumour at an early stage as it offers a high chance of a cure with a low amount of systemic side effects. However, tumours are often only discovered at an advanced, metastatic stage, when they are usually inoperable. For advanced-stage NSCLC, chemotherapy and radiotherapy were the only options until the advent of targeted therapy and immunotherapy. While chemotherapy and radiotherapy also have an unspecific, toxic effect on non-cancerous cells, targeted therapy is directed specifically against, for example, a mutated variant of a protein with ideally little to no effect on the wild-type protein and correspondingly far fewer side effects.

The concept of "oncogene addiction" describes the phenomenon where certain cancer cells become dependent on the continuous activity of a single oncogenic pathway or protein to

maintain their malignant properties[27]. Despite accumulating numerous mutations, these cancer cells rely predominantly on the sustained function of their driver oncogene, such as *EGFR* or *BRAF* in lung cancer to sustain their survival and proliferation. Experimental evidence from tumour models further supports this concept, showing that the acute inhibition of oncogene activity can induce cancer cell death through proliferative arrest, apoptosis, or differentiation[28,29]. The dependence of cancers on specific oncogenes creates a vulnerability that can be exploited therapeutically, as demonstrated by the dramatic tumour regressions and prolonged survival observed in patients treated with targeted therapies aiming at these oncogenes[30–32]

A model to explain the effects of oncogenic addiction in response to therapy is based on the 'oncogenic shock' concept. Oncogenes, especially RTKs such as EGFR, activate various signalling pathways, which mediate proliferation and pro-survival but also pro-apoptotic signals[33,34]. These opposing signals must be kept at a delicate balance in favour of the pro-survival signals to ensure the survival of the cancer cells. When inhibiting the oncogene using targeted therapy, the pro-survival signals vanish faster than their pro-apoptotic counterparts, thus leading to programmed cell death[33,34]**.**

During tumourigenic growth, numerous cellular processes are rewired, resulting in rapid proliferation leading to elevated cellular stress levels. This includes induction of DNA damage and replication stress, as well as metabolic, proteotoxic and oxidative stress.[35–37] Cancer cells have been shown to be more dependent on stress-reduction pathways than wild-type cells. Inhibition or depletion of key proteins in these pathways can cause stress overload and kill cancer cells specifically, as they have less buffering capacity than wild-type cells, thus opening a therapeutic window[35,37].

A subset of the non-oncogene addiction model is the concept of synthetic lethality. This describes the phenomenon whereby two genetic alterations that are harmless to cell viability when occurring separately are lethal to the cell when they occur together (**Figure 7**).

Prior to therapy, activating mutations in *EGFR* and *KRAS* are virtually mutually exclusive and thus do not occur in the same cancer. *In vitro* experiments demonstrated that cells with simultaneous expression of activating *EGFR* and *KRAS* mutations exhibited synthetic lethality, which could be rescued by inhibiting one of the two mutations[1]. Subsequent experiments demonstrated that the hyperactivation of the MAPK signalling pathway is the underlying cause of cell death in this context[2]. Petti et al. demonstrated that melanoma cells that concurrently express $BRAF^{V600E}$ and $NRAS^{Q61R}$ mutations undergo a process of cellular senescence and cell cycle arrest[38].

The concepts of oncogenic addiction and non-oncogene addiction of cancer cells explain why targeted therapy can be so effective for patients with tumours, and they provide the rationale

for developing novel therapeutic approaches tackling these "Achilles' heels". One of the first oncogenes to be targeted was EGFR in NSCLC with first-generation EGFR tyrosine kinase inhibitors (TKI) such as erlotinib and gefitinib, with clinical trials showing improved progression-free survival with fewer side effects compared to chemotherapy. A retrospective study by Howlader et al. showed that in patients in the United States, the incidence of NSCLC and, correspondingly, incidence-based mortality declined between 2006 and 2016[39]. Between 2013 and 2016, incidence-based mortality declined significantly more than incidence. This is explained by the approval of EGFR inhibitors erlotinib and afatinib against advanced NSCLC harbouring *EGFR*^{L858R} or *EGFR*^{del19} mutations by the U.S. Food and Drug Administration (FDA) in 2013 and the resulting benefit of treatment with targeted EGFR TKIs[39,40].

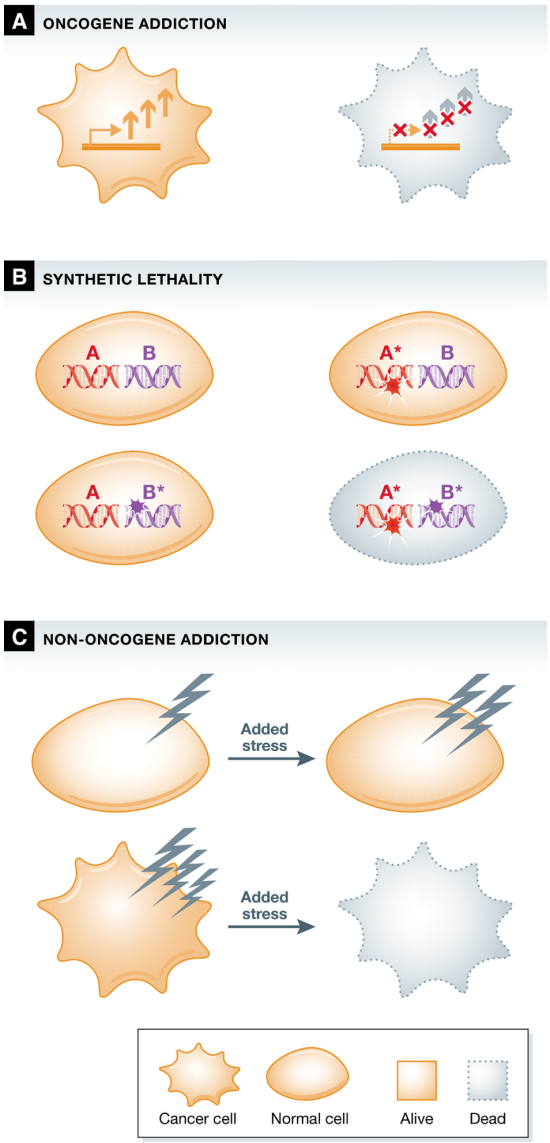

Figure 7. Schematic overview of the concepts of oncogene addiction, synthetic lethality and non-oncogene addiction. A) The cancer cell depends on oncogene-driven, persistent, and elevated cell signalling (symbolized by arrows) and succumbs to signal inhibition. B) Cancer cells are viable with either genetic alteration A* or B*, respectively. Co-existence of genetic alterations A* and B* have been shown to be synthetic lethal. C) Cancer cells exhibit

elevated stress levels compared to normal cells. Additional stress can be accommodated by normal cells, which possess the necessary resources to buffer it. However, cancer cells lack these resources and consequently experience stress levels that exceed a critical lethal threshold. (reproduced from Nagel, Semenova and Berns, 2016)[37]

2.5 Resistance mechanisms

In the context of EGFR-mutated LUAD, virtually all patients develop resistance upon targeted therapy. Drug resistance can be categorised into on-target and off-target resistance mechanisms. On-target mechanisms involve mutations or other alterations of the target protein that lead to an ongoing signal in the presence of the drug or prevent it from binding. Off-target mechanisms lead to an ongoing signal independent of the target gene, for example through acquired alterations downstream in the same or in parallel signalling pathways (**Figure 8**)[41].

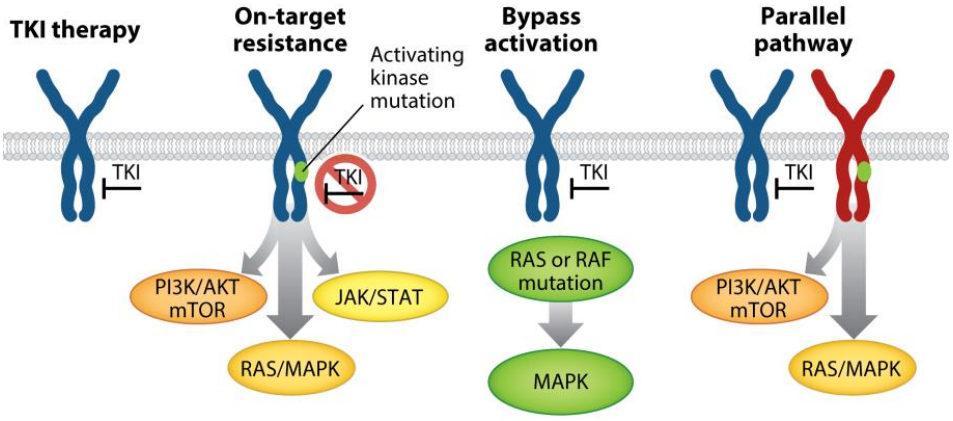

Figure 8. Mechanisms of acquired resistance following targeted therapy with EGFR-TKIs. Mutated *EGFR* is inhibited by a TKI. On-target resistance mutations prevent TKI binding and subsequent signaling in the downstream RAS-MAPK, PI3K-AKT-mTOR, and JAK/STAT pathways. Sustained signaling is enabled by mutations that bypass the inhibited oncogene in the pathway, such as RAS or RAF in the MAPK pathway. Alterations that cause alternative receptor tyrosine kinases to restore signaling in the oncogene-dependent cell through parallel pathways. (modified from Tulpule and Bivona, 2020)[41]

Acquired resistance to first-generation EGFR-TKIs is often caused by the *T790M* gatekeeper mutation in the adenosine triphosphate (ATP) binding pocket of EGFR, seen in 50–60% of relapsing patients[42,43]. Second-generation EGFR-TKIs, including afatinib and dacomitinib, covalently bind to EGFR, in contrast to first-generation EGFR-TKIs. Nevertheless, in the context of inhibiting $EGFR^{T790M}$, the results obtained *in vitro* and *in vivo* were comparable to those of first-generation EGFR-TKIs[44,45]The substitution of threonine for methionine at amino acid position 790 (*T790M*) impedes the binding of first- and second-generation TKIs due to steric hindrance caused by the larger methionine residue[43,46]. Third-generation EGFR-TKIs, such as osimertinib, were developed to overcome the *T790M* gatekeeper mutation. They form an irreversible covalent bond with the cysteine-797 residue in the ATP binding site of EGFR and avoid the steric clash with the gatekeeper.[47,48] These inhibitors demonstrated potent

activity against the *EGFR*^{T790M} mutation while exhibiting minimal inhibitory activity against the wild-type receptor[47]. In multiple large-scale clinical trials, osimertinib showed not only an effect in EGFR-TKI-pretreated patients with a *T790M* mutation but also superiority over chemotherapy and first-generation TKIs[48–51]. These results led to the approval of osimertinib as first-line therapy for EGFR-mutated NSCLC.

Unfortunately, similar to first- and second-generation EGFR TKIs, the cancer cells develop resistance after treatment with osimertinib. The *EGFR*^{C797S} mutation, which prevents covalent binding, is one of the most common alterations after second-line treatment, occurring in 10-26% of patients[49,52]. When osimertinib is applied as first-line therapy, *C797S* occurs in 7% of patients, alongside other on-target and off-target resistance mechanisms such as *MET* amplification, *BRAF* and *KRAS* mutations and *RET* fusions[16,52,53].

2.6 Aims of the work

Despite significant progress in targeted therapies, resistance and subsequent disease progression remain major challenges. A detailed understanding of the underlying resistance mechanisms is essential to identify potential vulnerabilities and improve therapeutic strategies. Building on observations that co-activation of EGFR and KRAS can induce synthetic lethality via MAPK pathway hyperactivation, it is plausible that other downstream mutations, such as *BRAF*^{V600E}, might elicit a similar effect.

The objective of this study is to provide a comprehensive molecular and phenotypic characterization of concurrent *EGFR* and *BRAF* mutations in LUAD. Firstly, the question of whether co-expression of *EGFR*^{del19} and *BRAF*^{V600E} mutations leads to synthetic lethality is investigated. The second aim is to address the question of how to overcome BRAF-mediated resistance to EGFR-TKI therapy.

To this end, cell culture-based models of EGFR-TKI resistance involving *EGFR*^{del19} and *BRAF*^{V600E} co-mutations are analysed and compared to cells harbouring only *EGFR*^{del19}. These models are implemented to perturb MAPK signalling using targeted inhibitors such as osimertinib (EGFR), vemurafenib (BRAF^{V600E}), and trametinib (MEK1/2). Combination treatments targeting the same pathway are evaluated for synergistic effects and their ability to overcome EGFR-TKI resistance. Findings from *in vitro* experiments are validated *in vivo* and complemented by RNA sequencing of E2F target genes and MAPK pathway responsive genes to assess the impacts of pathway perturbations on gene expression to better reflect clinical implications. As part of a comprehensive translational approach, all experiments are embedded in the context of a patient cohort exhibiting co-expression of *EGFR* and *BRAF* mutations either on initial diagnosis or as a resistance mechanism to EGFR-TKI therapy.

3. Publication

Clonal dynamics of *BRAF*-driven drug resistance in *EGFR*- mutant lung cancer

Diana Schaufler*, David F. Ast*, Hannah L. Tumbrink, Nima Abedpour, Lukas Maas, Ayla E. Schwäbe, Inga Spille, Stefanie Lennartz, Jana Fassunke, Mihaela Aldea, Benjamin Besse, David Planchard, Lucia Nogova, Sebastian Michels, Carsten Kobe, Thorsten Persigehl, Theresa Westphal, Sophia Koleczko, Rieke Fischer, Jan-Phillip Weber, Janine Altmüller, Roman K. Thomas, Sabine Merkelbach-Bruse, Oliver Gautschi, Laura Mezquita, Reinhard Büttner, Jürgen Wolf, Martin Peifer, Johannes Brägelmann[#], Matthias Scheffler[#] and Martin L. Sos[#]

(* co-first authors, # co-corresponding authors)

npj | Precision Oncology

www.nature.com/npjprecisiononcology

ARTICLE OPEN

Check for updates

Clonal dynamics of *BRAF*-driven drug resistance in *EGFR*-mutant lung cancer

Diana Schaufler[1,14], David F. Ast[2,3,4,14], Hannah L. Tumbrink[2,3], Nima Abedpour[3,5], Lukas Maas[3], Ayla E. Schwäbe[2,3], Inga Spille[2,3], Stefanie Lennartz[2,3], Jana Fassunke[6], Mihaela Aldea[7], Benjamin Besse[7], David Planchard[7], Lucia Nogova[1], Sebastian Michels[1], Carsten Kobe[8], Thorsten Persigehl[9], Theresa Westphal[1], Sophia Koleczko[1], Rieke Fischer[1], Jan-Phillip Weber[1], Janine Altmüller[10], Roman K. Thomas[3,6,11], Sabine Merkelbach-Bruse[6], Oliver Gautschi[12], Laura Mezquita[13], Reinhard Büttner[6], Jürgen Wolf[1], Martin Peifer[3], Johannes Brägelmann[2,3,4,5]✉, Matthias Scheffler[1]✉ and Martin L. Sos[2,3,5]✉

Activation of MAPK signaling via *BRAF* mutations may limit the activity of EGFR inhibitors in *EGFR*-mutant lung cancer patients. However, the impact of *BRAF* mutations on the selection and fitness of emerging resistant clones during anti-EGFR therapy remains elusive. We tracked the evolution of subclonal mutations by whole-exome sequencing and performed clonal analyses of individual metastases during therapy. Complementary functional analyses of polyclonal *EGFR*-mutant cell pools showed a dose-dependent enrichment of $BRAF^{V600E}$ and a loss of EGFR inhibitor susceptibility. The clones remain stable and become vulnerable to combined EGFR, RAF, and MEK inhibition. Moreover, only osimertinib/trametinib combination treatment, but not monotherapy with either of these drugs, leads to robust tumor shrinkage in *EGFR*-driven xenograft models harboring $BRAF^{V600E}$ mutations. These data provide insights into the dynamics of clonal evolution of *EGFR*-mutant tumors and the therapeutic implications of *BRAF* co-mutations that may facilitate the development of treatment strategies to improve the prognosis of these patients.

npj Precision Oncology (2021)5:102 ; https://doi.org/10.1038/s41698-021-00241-9

INTRODUCTION

Targeted treatment of epidermal growth factor receptor (*EGFR*)-mutant non-small cell lung cancer (NSCLC) is a landmark for rational therapy addressing molecular vulnerabilities[1]. Treatment with first- and second-generation EGFR tyrosine kinase inhibitors (TKIs) markedly improved the clinical outcome of patients with advanced *EGFR*-mutant NSCLC[2–5]. Currently, osimertinib is the only third-generation EGFR inhibitor approved for the sequential treatment of patients with acquired $EGFR^{T790M}$ resistance mutation occurring after first- and second-generation TKIs[6,7]. In addition, osimertinib became the new standard-of-care in the first-line treatment of patients with *EGFR*-mutant NSCLC[8,9].

Despite the clinical efficacy of osimertinib in the first- and second-line treatment of *EGFR*-mutant NSCLC, drug resistance with disease progression is inevitable[10–18]. Various *EGFR*-dependent and *EGFR*-independent resistance mechanisms have been identified including $EGFR^{C797S}$ and $EGFR^{G724S}$ mutations, *MET*/*HER2* amplification, activation of the RAS–mitogen-activated protein kinase (MAPK) or RAS–phosphatidylinositol 3-kinase (PI3K) pathways, new fusions, and histological transformation. RAS–MAPK pathway aberrations that are known to confer resistance to osimertinib include *BRAF*, *NRAS*, and *KRAS* mutations[10,19,20]. *BRAF* mutations occur in 2–4% of NSCLC patients and the vast majority are localized in the kinase domain, including the most common mutation $BRAF^{V600E}$. *BRAF* mutations can be categorized into three classes based on their ability to act as monomers or dimers and based on their kinase activity. $BRAF^{V600E}$ mutations represent class I mutations that, similarly to class II *BRAF* mutations (*RAS*-independent), result in activation of the BRAF kinase and the MAPK pathway (gain of function). Class III *BRAF* mutations (*RAS*-dependent) result in an impaired BRAF kinase activity and amplify ERK signaling depending on upstream activating signals (e. g. *RAS* activating mutations, *NF1* tumor suppressor deletion)[21]. All classes of *BRAF* mutations are recognized as oncogenic driver mutations, yet only $BRAF^{V600E}$ mutations represent clinically actionable drug targets in cancer patients[22,23].

$BRAF^{V600E}$ mutations have been identified as a resistance mechanism to osimertinib in roughly 3% of cases with *EGFR*-mutant lung cancer, with or without concurrent $EGFR^{T790M}$ mutation[10,19,20]. Several combination therapies have been proposed for *BRAF* resistance in *EGFR*-mutant lung cancer, but an integrated genomic analysis of these tumors is lacking and precludes an optimization of therapeutic regimen[24–27]. Furthermore, the current understanding of the clonal evolution of *EGFR*-mutant cells that concomitantly acquire *BRAF* mutations during anti-EGFR therapy remains limited.

[1]University of Cologne, Faculty of Medicine and University Hospital Cologne, Department I of Internal Medicine, Center for Integrated Oncology Aachen Bonn Cologne Duesseldorf, Network Genomic Medicine, Lung Cancer Group Cologne, Cologne, Germany. [2]University of Cologne, Faculty of Medicine and University Hospital Cologne, Institute of Pathology, Molecular Pathology, Cologne, Germany. [3]University of Cologne, Faculty of Medicine and University Hospital Cologne, Department of Translational Genomics, Cologne, Germany. [4]Mildred Scheel School of Oncology, Faculty of Medicine and University Hospital Cologne, University of Cologne, Cologne, Germany. [5]University of Cologne, Faculty of Medicine and University Hospital Cologne, Center for Molecular Medicine Cologne, Cologne, Germany. [6]University of Cologne, Faculty of Medicine and University Hospital Cologne, Institute of Pathology, Network Genomic Medicine, Cologne, Germany. [7]Department of medical oncology, Thoracic Group, Gustave Roussy, Villejuif, Paris Sud University Orsay, Paris, France. [8]University of Cologne, Faculty of Medicine and University Hospital Cologne, Department of Nuclear Medicine, Cologne, Germany. [9]University of Cologne, Faculty of Medicine and University Hospital Cologne, Institute of Diagnostic and Interventional Radiology, Cologne, Germany. [10]Cologne Center for Genomics, University of Cologne, Cologne, Germany. [11]DKFZ, German Cancer Research Center, German Cancer Consortium (DKTK), Heidelberg, Germany. [12]University of Bern and Cantonal Hospital of Lucerne, Lucerne, Switzerland. [13]Medical Oncology Department, Hospital Clinic, Laboratory of Translational Genomics and Targeted therapies in Solid Tumors, IDIBAPS, Barcelona, Spain. [14]These authors contributed equally: Diana Schaufler, David F. Ast. ✉email: johannes.braegelmann@uni-koeln.de; matthias.scheffler@uk-koeln.de; martin.sos@uni-koeln.de

Published in partnership with The Hormel Institute, University of Minnesota

npj nature partner journals

The Hormel Institute University of Minnesota

Within the present study, we aimed for a comprehensive and translational approach to systematically characterize the role of co-occurring *EGFR*/*BRAF* mutations in patients with advanced lung adenocarcinoma.

RESULTS

Targeting *BRAF*-driven resistance in *EGFR*-mutant lung cancer

To characterize the role of *BRAF* mutations in the context of druggable *EGFR* mutations, data of eligible patients from several centers were analyzed (see "Methods"). This led to the identification of 15 patients with lung adenocarcinoma harboring activating *EGFR* mutations and co-occurring *BRAF* mutations (Fig. 1a, Table 1). In five cases, *EGFR* and *BRAF* mutations were detected at the time of initial diagnosis, whereas in ten patients, *BRAF* mutations were acquired after anti-EGFR therapy (Table 1). In eight patients, *BRAF* mutations occurred after osimertinib treatment, in one patient after gefitinib treatment, and in one patient after afatinib treatment. The treatment history of these ten patients before the detection of acquired *BRAF* mutations is outlined in Supplementary Fig. 1. The median duration of time elapsed from diagnosis of *EGFR*-mutant lung cancer to the detection of acquired *BRAF* mutation was 33.8 months (95% CI: 9.0–99.1 months) (Fig. 1b). Six patients were evaluable for analysis of subsequent treatment and outcome after detection of acquired *BRAF* mutation (Fig. 1c, Table 2). Median overall survival (OS) for these six patients after detection of *BRAF*-driven acquired resistance was 7.8 months (95% CI: 5.1–10.5 months; Fig. 1c). Of which, four patients (P12–P15) presenting with acquired activating $BRAF^{V600E}$ and $BRAF^{K601E}$ (gain of function) mutations received either osimertinib and bevacizumab ($n = 2$), osimertinib and chemotherapy ($n = 1$), or chemotherapy plus bevacizumab ($n = 1$) as the next line of treatment after detection of the *BRAF* mutation (Table 2). In the Cologne cohort, we detected 26/1951 co-occurrences of *EGFR* and *BRAF* mutations (1.3%) but narrowed it down to clearly activating *EGFR* mutations. In the Paris cohort, we detected 4/184 co-occurrences of *EGFR* and *BRAF* mutations (2.2%). Overall, our data show that *BRAF* mutations represent a resistance mechanism in a relevant proportion of *EGFR*-mutant patients, warranting further investigation of the underlying clinical and evolutionary dynamics.

Next, we selected two patients (P01, P04) who acquired $BRAF^{V600E}$ mutation under osimertinib treatment to evaluate the safety and efficacy of various drug combinations including EGFR, RAF, MEK, or MET inhibitors, chemotherapy, or bevacizumab (Table 2, Fig. 1d, Supplementary Fig. 2a). We chose functional imaging by FDG-PET for (early) metabolic response evaluation during our investigational conduct (Supplementary Table 1) and monitored treatment-related adverse events that were predominantly of low grade and manageable (Supplementary Table 2). Osimertinib treatment was initiated and carried out for 16 months in P01 and 7 months in P04 before the detection of progressive disease. While in P01 $EGFR^{T790M}$ mutation was sustained, in P04, we observed a loss of $EGFR^{T790M}$ mutation. Both patients started with dabrafenib and trametinib, which in both cases did not lead to a confirmed metabolic response. Both patients underwent a rebiopsy of progressive lesions and started immediately with osimertinib and dabrafenib. In P01, the rebiopsy revealed an $EGFR^{del19}$ mutation, loss of $EGFR^{T790M}$, no $BRAF^{V600E}$ mutation and an intermediate-level *MET* amplification (GCN 5.58, FISH). Subsequent doublet combinations of osimertinib plus dabrafenib and afatinib plus crizotinib showed either primary refractory disease or metabolic responses that could not be confirmed in the next scans. In contrast, the triple combination of osimertinib, dabrafenib, and trametinib led to a prolonged metabolic response and clinical benefit (Supplementary Table 1, Table 2). In P04, doublet combinations of osimertinib and dabrafenib led only to a short metabolic response not confirmed in the next scan, and with the addition of trametinib, we then observed a marked metabolic response in the primary lung tumor but not in the hepatic metastases. Rebiopsy of the hepatic lesions revealed an $EGFR^{del19}$ mutation with T790M and C797S resistance mutations in *cis* and no *BRAF* mutation. Treatment was thus changed to osimertinib plus chemotherapy/transarterial chemoembolization due to progressive liver metastases. The patient, unfortunately, died a year after detection of $BRAF^{V600E}$ resistance. Thus, biopsy-guided mutational profiling in conjunction with FDG-PET imaging can guide effective combination therapies to overcome resistance in these patients.

To investigate the clonal dynamics during the development of resistance, we performed whole-exome sequencing (WES) of biopsies from multiple time points and different metastatic sites obtained from P01 to P04 (Fig. 1d–i (P04), Supplementary Fig. 2 (P01)). For patient P01 WES could be performed on the primary tumor and two metastatic samples (Supplementary Fig. 2), while insufficient tissue, unfortunately, precluded analysis of the *BRAF*-mutant metastasis. Pairwise clustering based on the cancer cell fractions of the mutations (CCFs, i.e. frequency of occurrence in cancer cells after adjustment for purity, ploidy, and copy number (CN)[28] revealed a high proportion of private mutations, while only a few mutations (e.g., $EGFR^{del19}$) were clonal in all samples (Supplementary Fig. 2b–d). Due to the sequencing quality, an intra-biopsy heterogeneity analysis was not undertaken, but phylogenetic tree analysis between biopsies indicated a branched evolution during resistance development (Supplementary Fig. 2e). Interestingly, a common ancestor gave rise to the pleural upper lung lobe metastasis and clones subsequently developing into the pleural metastasis and the primary tumor. In accordance with this branching model, the CN profiles show shared alterations between all three available samples, but also CN segments exclusive to just one or a pair of samples (Supplementary Fig. 2f). Our data indicate early branching during tumor development and is in accordance with a scenario where resistant cells develop in parallel to the primary tumor even before treatment pressure is applied.

For patient P04 WES was performed on a peritoneal metastasis that occurred during initial inhibitor treatment ($EGFR^{del19}$ and $EGFR^{T790M}$), a liver metastasis 6 months after treatment had been switched to osimertinib ($EGFR^{del19}$ and $BRAF^{V600E}$) and a rebiopsy of the same liver lesion at progressive disease under dabrafenib and trametinib treatment ($EGFR^{del19}$ and $BRAF^{V600E}$) (Fig. 1d). Comparative pairwise CCF-based clustering showed only a few mutations to be shared between the peritoneal biopsy and the first liver biopsy (e.g., $EGFR^{del19}$), while the majority was private for each one of metastases (e.g., $EGFR^{T790M}$ and $BRAF^{V600E}$, respectively) (Fig. 1e). In contrast, almost all mutations were found to be shared between both biopsies of the liver lesion (Fig. 1f). Subclonal composition analysis of the peritoneal metastasis revealed two subclones (C1 60%, C3 40%), while the liver metastases presented with one dominant clone each (Fig. 1g).

For subsequent phylogenetic analyses, a founder clone C0 was derived based on the mutations shared by all biopsies since the material of the primary tumor was unavailable for WES. Tracking the genomic development from C0 indicated a branched evolution diverging towards the peritoneal metastasis carrying $EGFR^{T790M}$ with its first subclone C1, which further spawned a new subclone C3 present in the same biopsy (Fig. 1h). The liver metastasis appeared to have developed from C0 independently of the peritoneal metastasis by acquiring the $BRAF^{V600E}$ mutation (C2). The rebiopsy of that lesion showed a distinguishable clone C4 which only carried one additional non-synonymous mutation of unknown biological relevance indicating a high degree of genetic similarity (Fig. 1h). In addition, genetic similarities between lesions were quantified to gain further insight into the clonal evolution toward therapy resistance (see Supplementary Material for further details). This analysis supports a branched evolution

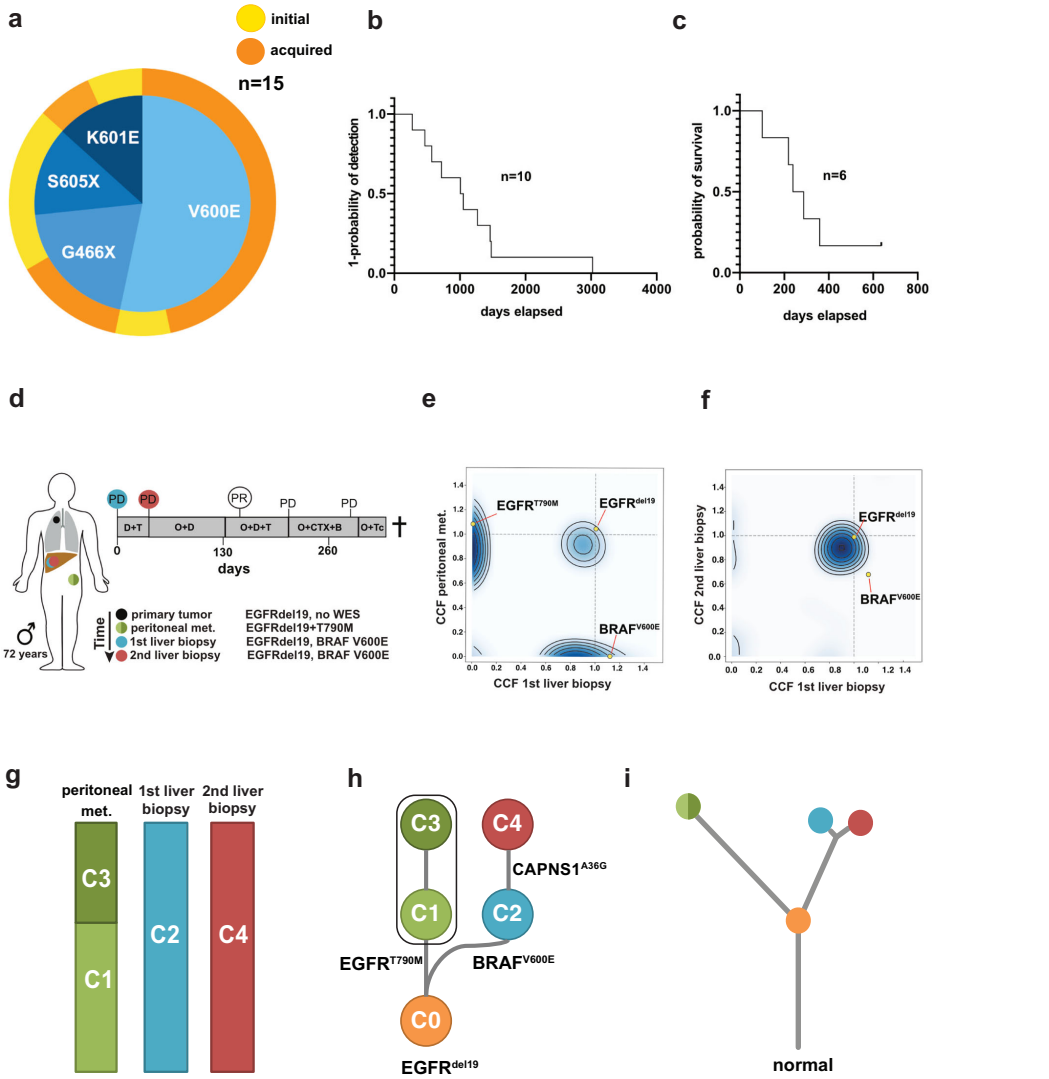

Fig. 1 Clinicopathological characteristics for the study cohort and clonal evolution. a Spectrum and distribution of *BRAF* co-mutations in patients with *EGFR*-mutant lung adenocarcinoma. **b** Kaplan–Meier curve of the time elapsed from the detection of the *EGFR* mutation until the detection of the acquired *BRAF* mutation (as events) in days. **c** Kaplan–Meier curve of overall survival for patients P01, P04, P12–P15 that were available for survival analysis. **d** Overview of the biopsies and key molecular findings by NGS for patient P04. Flow chart (top right) summarizes lines of therapy approaches overtime after the acquisition of $BRAF^{V600E}$ mutation. **e**, **f** Clustering of WES-derived mutations based on their CCFs between pairs of tumor biopsies to detect clusters of shared clonal and private mutations. Candidate mutations in *EGFR* and *BRAF* are highlighted. **g** Subclonal composition in individual biopsies indicating two subclones (C1, C3) in the peritoneal metastasis and single clones in the liver metastases. **h** Clonal evolution of reconstructed cell populations presented as a phylogenetic tree. The computationally inferred most common ancestor C0 is common to all subsequent clones and highlighted mutations are present in descendent clones. **(i)** Visualization of evolutionary genetic distances between normal tissue and longitudinal biopsies. WES whole-exome sequencing, NGS next-generation sequencing, PD progressive disease, PR partial response, D + T dabrafenib+trametinib, O + D(+T) osimertinib+dabrafenib(+trametinib), O + CTX + B osimertinib+chemotherapy+bevacizumab, O + Tc TACE osimertinib+transarterial chemoembolization, C clone, CCF cancer cell fraction.

Table 1. Clinicopathological characteristics for the study cohort.

Patient ID	Sex	Age	Biopsy	*EGFR* mutation	*BRAF* mutation		Co-mutations	
01	F	70	TB	E746_A750del, T790M	V600E	Class I	Acquired (osimertinib)	Persistent T790M
02	F	71	TB	E746_A750del, T790M	S605C	Not classified	Initial	TP53 R273H
03	M	61	TB	L858R	K601E	Class II	Initial	DDR2 R279M
04	M	72	TB	E746_A750del, T790M	V600E	Class I	Acquired (osimertinib)	loss of T790M
05	M	77	TB	L861Q	G466A	Class III	Acquired (afatinib)	ERBB2 G815A, TP53 S166*
06	M	66	TB	L858R, V834L	V600E	Class I	Acquired (osimertinib)	loss of *EGFR* mutations
07	F	84	TB	L858R	V600E	Class I	Initial	–
08	F	74	TB	L858R	G466E	Class III	Acquired (gefitinib)	–
09	M	50	TB	E746_A750del	V600E	Class I	Acquired (osimertinib)	CCDC6-RET
10	F	67	TB	L747_P753delinsS	G466E	Class III	Initial	*KRAS* A59E
11	F	75	TB	E746_A750del	S605N	Not classified	Initial	–
12	F	61	LB	E746_A750del, 790M, C797S, C797G	V600E	Class I	Acquired (osimertinib)	TP53 splice
13	M	50	LB	L747_S752del	K601E	Class II	Acquired (osimertinib)	TP53 R248G
14	F	70	TB	L858R, T790M, C797S	V600E	Class I	Acquired (osimertinib)	TP53 K120E, BRCA S237Y (VUS)
15	M	52	TB	L747_A750delinsP T790M, C797G	V600E	Class I	Acquired (osimertinib)	CTNNB1 S37C, ATM R1437K (VUS)

Patients with lung adenocarcinoma harboring activating *EGFR* mutations and co-occurring *BRAF* mutations were collected from three different cancer centers. Class I and class II (RAS-independent) *BRAF* mutations result in activation of the BRAF kinase and the MAPK pathway. Class III (RAS-dependent) *BRAF* mutations result in impaired BRAF kinase activity and amplify ERK signaling based upon upstream activating signals. $BRAF^{S605C/N}$ mutations (variants) lie within the kinase domain of the BRAF protein, they are not yet functionally classified. TB tissue biopsy, LB liquid biopsy.

Table 2. Systemic treatment lines and outcome evaluable for six patients after detection of the acquired *BRAF* mutation.

Patient ID	*BRAF* mutation	Time to detection of *BRAF* mutation after diagnosis (months)	Treatment after detection of *BRAF* mutation	TTD (days)	OS (days)	Outcome
01	V600E (Class I)	96	Dabrafenib+trametinib (1 L)	74	636	Alive
			Osimertinib+dabrafenib (2 L)	27		
			Afatinib+crizotinib (3 L)	65		
			Osimertinib+dabrafenib + (4 L) trametinib	288		
			Osimertinib+bevacizumab (5 L)	53		
			Afatinib+crizotinib (6 L)	105		
			Osimertinib+dabrafenib + (7 L) trametinib	na		
04	V600E (Class I)	47	Dabrafenib+trametinib (1 L)	38	287	Deceased
			Osimertinib+dabrafenib (2 L)	93		
			Osimertinib+dabrafenib + (3 L) trametinib	77		
			Osimertinib+carboplatin + (4 L)	75		
			Pemetrexed+bevacizumab osimertinib+TACE (5 L)	na		
12	V600E (Class I)	38	Carboplatin+paclitaxel + (1 L) bevacizumab	68	101	Deceased
13	K601E (Class II)	26	Osimertinib+paclitaxel (1 L)	50	239	Deceased
14	V600E (Class I)	34	Osimertinib+bevacizumab (1 L), carboplatin +gemcitabine (2 L)	92, 40	359	Deceased
15	V600E (Class I)	51	Osimertinib+bevacizumab (1 L) carboplatin +paclitaxel + (2 L) bevacizumab	57, 163	219	Deceased

$BRAF^{V600E}$ and $BRAF^{K601E}$ mutations result in an increased BRAF kinase activity. See also Fig. 1c for the Kaplan–Meier curve of OS. TTD time-to-treatment discontinuation, OS overall survival: time from acquired resistance (date of biopsy) until death/last day of follow-up, TACE transarterial chemoembolization.

trajectory model with a common ancestor giving rise to the peritoneal metastasis and liver metastases (Fig. 1i). While the peritoneal metastasis and liver metastases are not closely related, only minor changes occurred between the first and second biopsy of the liver lesion (Fig. 1i). Accordingly, the CN landscape is very similar between the peritoneal metastasis and liver metastases, but almost identical between both liver biopsies (Supplementary Fig. 3). This highlights that the different metastases and resistance mechanisms ($EGFR^{T790M}$ and $BRAF^{V600E}$, respectively) developed independently from a common ancestral clone rather than in a linear relationship. Also, the remarkably high similarity between both liver biopsies indicates that selection pressure did not give rise to a highly distinct new subclone, potentially due to the lack of an EGFR inhibitor in the combination treatment. However, it may also be due to resistance to anti-BRAF therapy already being present in the clone C2 that propagates to C4 or may have a non-genomic basis not detectable by WES.

For a third patient (P14) we obtained a biopsy at the time of progression under osimertinib treatment (Supplementary Fig. 4a). WES of this biopsy showed the presence of several oncogenic *EGFR* mutations, namely L858R, T790M, and C797S (Supplementary Fig. 4b). All of those mutations were clonal, the T790M and C797S mutations are in agreement with previously described resistance mechanisms to EGFR inhibitors. Interestingly, we also detected a $BRAF^{V600E}$ mutation (Supplementary Fig. 4b, Table 1). In contrast to the *EGFR* mutations, the *BRAF* mutation was subclonal and may thus indicate the branching of a newly developing subclone. This further highlights the complexity of disease resistance, which may incorporate several mechanisms of resistance development in parallel. Overall, the clonal analyses highlight that a process of branched evolution underlies resistance to targeted treatments in patients with *EGFR*-mutant tumors and may give rise to various independent resistance mechanisms.

Resistance through the selection of $BRAF^{V600E}$-positive clones

To functionally validate our clinical observations, we overexpressed $BRAF^{V600E}$ in $EGFR^{del19}$-mutant PC9 cells. To compare $BRAF^{V600E}$-mediated effects to upstream activation of MAPK signaling, we generated cells expressing $NRAS^{Q61K}$, a mutation reported in preclinical models of acquired EGFR-inhibitor resistance[16,19]. In a polyclonal pool of PC9 cells stably expressing $BRAF^{V600E}$ or $NRAS^{Q61K}$, only modest activation of the MAPK signaling was detected as determined by immunoblotting of phospho-ERK (Fig. 2a). However, residual phospho-ERK-levels after osimertinib treatment were detected only in cells with $BRAF^{V600E}$ or $NRAS^{Q61K}$ overexpression but not in control PC9 empty vector (EV) cells. During 7-14 day treatment the insufficient inhibition of MAPK signaling translated into the outgrowth of osimertinib-resistant clones in cells expressing $BRAF^{V600E}$ or $NRAS^{Q61K}$ (Fig. 2b, c). In line with this observation, only ≤0.3% of PC9 (EV) cells were found to be able to give rise to colonies during increasing doses of osimertinib treatment (Fig. 2d). However, overexpression of $BRAF^{V600E}$ or $NRAS^{Q61K}$ significantly enhanced the pool of cells with the capacity to outgrow during therapy to 5.2% (*BRAF*) and 4.5% (*NRAS*) or less in a dose-dependent manner (Fig. 2d).

The next question was whether the enrichment of cells with high $BRAF^{V600E}$ or $NRAS^{Q61K}$ expression would have an impact on EGFR inhibitor sensitivity. Therefore, polyclonal $PC9^{BRAF\text{-}V600E}$ and $PC9^{NRAS\text{-}Q61K}$ cells were preselected either with 10 nM ($PC9^{BRAF/NRAS}$ OS 10 nM) or 100 nM ($PC9^{BRAF/NRAS}$ OS 100 nM) of osimertinib over the course of >30 days. Using RT-PCR a dose-dependent elevation of RNA levels of the respective resistance alleles was found in $PC9^{BRAF}$ OS and $PC9^{NRAS}$ OS cells after osimertinib selection (Fig. 2e, f). Osimertinib-preselected cells exhibited a higher induction of $BRAF^{V600E}$ expression (9.39-fold) than $NRAS^{Q61K}$ expression (4.25-fold, $p = 0.036$). Accordingly, untreated osimertinib-preselected cells with high $BRAF^{V600E}$ expression displayed stronger phospho-ERK staining when compared to $NRAS^{Q61K}$ (Fig. 2g). Both osimertinib-preselected $PC9^{BRAF\text{-}V600E}$ and $PC9^{NRAS\text{-}Q61K}$ cells showed higher levels of sustained phospho-ERK during osimertinib treatment (Fig. 2g) and a higher degree of resistance in viability assays compared to non-selected cells (Fig. 2h). A similar degree of resistance was observed against the EGFR inhibitors erlotinib or afatinib (Supplementary Fig. 5a, b) but not against the non-specific, chemotherapeutic cisplatin (Supplementary Fig. 5c).

To further substantiate our data in an independent model, $BRAF^{V600E}$ was overexpressed in the $EGFR^{del19}$-mutant HCC827 cell line. Again, a dose-dependent induction of resistance thro ugh osimertinib-preselection was observed in polyclonal $HCC827^{BRAF\text{-}V600E}$ cell pools (Supplementary Fig. 5d). These findings are in line with our clinical observations and previous cases that identified *BRAF*-mediated resistance in *EGFR*-mutant tumors during anti-EGFR therapy. Our results suggest that *BRAF*-mutant clones are enriched through EGFR-directed therapy in *EGFR*-mutant adenocarcinoma.

Overcoming $BRAF^{V600E}$-mediated resistance in *EGFR*-mutant cells

Previous studies have found that concomitant *KRAS* and *EGFR* mutations may increase the cell death rate of adenocarcinoma cells through hyperactivation of ERK signaling[29,30]. We tested whether the activation of MAPK signaling via $BRAF^{V600E}$ may have a similar effect in *EGFR*-mutant PC9 cells. To this end, the cell proliferation of $PC9^{BRAF\text{-}V600E}$ and $PC9^{NRAS\text{-}Q61K}$ was measured over 5 days, but no major differences were observed compared to EV cells (Fig. 3a). We also did not detect any differences in the basal cell death rate between cell lines (Supplementary Fig. 6a). Consequently, cells with high expression of mutant *BRAF*/*NRAS* did not get counter-selected after the withdrawal of osimertinib (Fig. 3b, c).

Next, we tested combination therapies by targeting EGFR and MAPK signaling individually in $PC9^{BRAF\text{-}V600E}$ and $PC9^{NRAS\text{-}Q61K}$ cells (Fig. 3d). Both MEK inhibition and BRAF inhibition, as monotherapy, had a limited effect on the viability of $PC9^{BRAF\text{-}V600E}$ mutant cells (Supplementary Fig. 6b, c). In contrast, the combination of osimertinib and MEK or BRAF inhibition effectively prevented the outgrowth of colonies (Fig. 3d). To further validate our previous findings on a transcriptional level, we performed RNA sequencing of PC9 (EV), $PC9^{BRAF\text{-}V600E}$, and $PC9^{BRAF\text{-}V600E}$ OS 100 nM cells treated with osimertinib, trametinib, a combination of both or control for 48 h (see Supplementary Material). As expected, a principal component analysis showed that osimertinib monotherapy had strong effects only on $PC9^{BRAF\text{-}V600E}$ cells, while trametinib plus osimertinib comparably impacted both $PC9^{BRAF\text{-}V600E}$ and $PC9^{BRAF\text{-}V600E}$ OS 100 nM cells (Supplementary Fig. 6d). We next clustered samples based on the expression of E2F target genes to assess the impact on cell cycle-related gene expression as a surrogate marker for the cytotoxic effects of the given perturbation (Fig. 3e). In this analysis, the strongest down-regulation of E2F genes was present in the group of cell line/treatment combinations that led to reduced cell numbers in crystal violet assays (Fig. 3d). Repression of E2F target genes was lower in unselected $PC9^{BRAF\text{-}V600E}$ cells with osimertinib compared to PC9 EV cells or compared to combination treatment (Fig. 3d). This indicates the limited efficacy of osimertinib monotherapy treatment if a *BRAF* mutation is present even without prior selection and supports the use of combination treatment. Furthermore, in $PC9^{BRAF\text{-}V600E}$ OS 100 nM cells the expression of MAPK pathway responsive genes was only perturbed during osimertinib and trametinib treatment (Supplementary Fig. 7a)[31]. Next, we assessed the synergy between osimertinib and trametinib, using ZIP-based synergy analysis, and found a strong

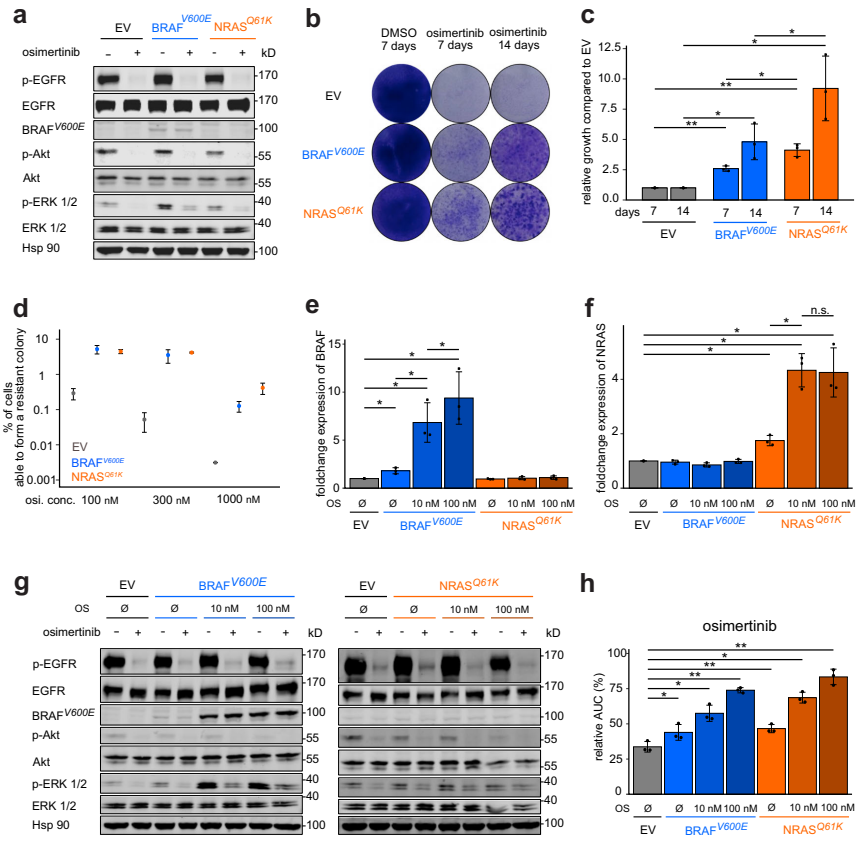

Fig. 2 Selection of *BRAF*^{V600E}-positive clones in *EGFR*-mutant cells. a Immunoblotting of PC9 cells expressing the annotated constructs, treated with (+) or without (−) osimertinib (48 h). Hsp90 is used as a loading control. **b** Clonogenicity assays of PC9 derived cell lines treated with osimertinib for 7 and 14 days or DMSO control for 7 days are displayed. **c** Quantitative analysis of (**b**) normalized to PC9 (EV). **d** Limited dilution assay of PC9-derived cell lines treated for 21 days before analysis. **e**, **f** qRT-PCR analysis of mRNA expression in **e** *BRAF* and **f** *NRAS* in PC9 derived cell lines normalized to EV. **g** Immunoblotting of PC9 cells expressing the annotated constructs that were treated as in (**a**). **h** Viability curves of PC9 cells expressing the annotated constructs treated with osimertinib (72 h) are shown. The relative area under the curve (AUC) in % compared to a theoretical non-responding AUC. Error bars indicate mean ± SD. Two-tailed paired *t* tests, $^{***}p < 0.001$, $^{**}p < 0.01$, $^{*}p \leq 0.05$, $^{n.s.}p > 0.05$. *EGFR* epidermal growth factor receptor, *BRAF* B-rapidly accelerated fibrosarcoma, *NRAS* neuroblastoma rat sarcoma, EV empty vector.

synergy that correlated with the expression of BRAF-V600E in PC9 cells (Fig. 3f, see Methods). The calculated synergy score for osimertinib and vemurafenib was limited and we found an antagonism for the combination of trametinib and vemurafenib inhibition in PC9$^{BRAF\text{-}V600E}$ mutant cells (Supplementary Fig. 7b, c). Finally, using a three-fold titration matrix, we observed a considerably low synergy for osimertinib and vemurafenib treatment compared to osimertinib and trametinib treatment, which was not further increased in a triple combination by adding vemurafenib (Supplementary Fig. 7d). In accordance with the synergy results, osimertinib with trametinib in contrast to osimertinib alone resulted in full inhibition of phospho-ERK signaling. Vemurafenib did not fully abrogate the sustained phospho-ERK signaling, as it also hyperactivated phospho-ERK as monotherapy, most likely due to the paradoxical effect on the endogenous wild type BRAF kinase (Fig. 3g)[32]. To further validate our in vitro results, we performed an in vivo study with xenografts implanted with PC9$^{BRAF\text{-}V600E}$ cells that were preselected for high *BRAF*^{V600E} expression. Once the mice developed tumors, we started with the treatment regimen consisting of vehicle, osimertinib, trametinib or the combination of osimertinib and trametinib for 21 days (Fig. 3h). Compared to vehicle treatment, trametinib did not significantly decrease tumor volume, and osimertinib monotherapy led to a measurable tumor growth reduction. However, only, combination therapy led to robust tumor shrinkage in these xenografts (Fig. 3h). Thus, our in vivo data largely reflects our in vitro findings and suggests that combination therapy is necessary to induce substantial tumor shrinkage in tumors harboring activating *EGFR* and *BRAF* mutations. Of importance, none of the mice in the individual treatment arms experienced weight loss (Supplementary Fig. 7e) or any other severe treatment-associated side effects.

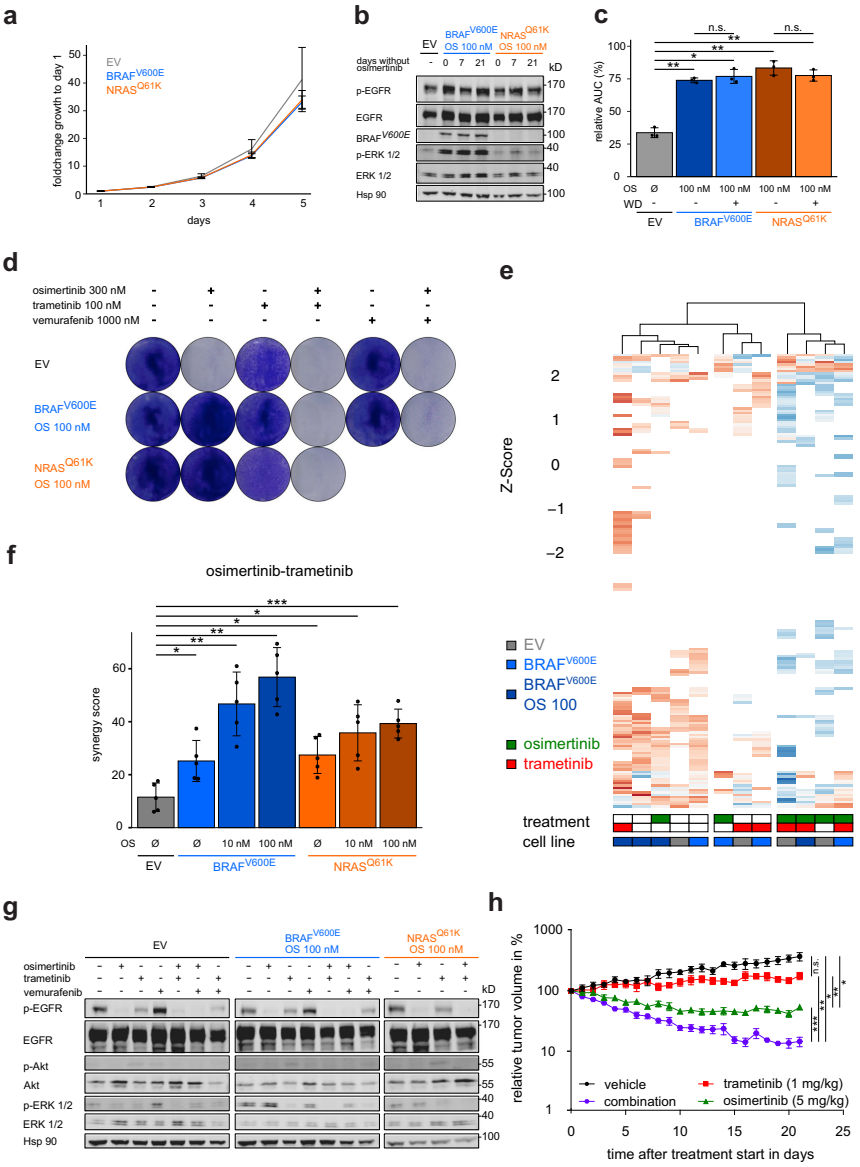

DISCUSSION

Osimertinib replaced other EGFR inhibitors in the early lines of therapy. This development had a major impact on the resistance profiles and development of effective salvage therapies[10–15,18,33]. The activation of MAPK signaling seems to play a more prominent role in patients' progressive on third-generation EGFR inhibitors when compared to first- and second-generation EGFR inhibitors[11,16,19,20,34]. Our comprehensive genomics study of *EGFR*-mutant patients with co-occurring *BRAF* mutations provides insights into the evolution of MAPK-driven resistance and its impact on *EGFR*-directed treatment.

Our combination of longitudinal clinical and genomic analyses provides insight into the subclonal heterogeneity of the individual tumors and corresponding metastases during resistance evolution. Our clonality analyses revealed that resistance to osimertinib (initiated at detection of $EGFR^{T790M}$ mutation) and subsequent

Fig. 3 Overcoming *BRAF*^{V600E}-mediated resistance in *EGFR*-mutant cells. a Growth series of PC9 derived cell lines counted for 5 days every 24 h (see Methods). **b** Immunoblotting of PC9$^{BRAF\text{-}V600E}$ OS 100 nM, PC9$^{NRAS\text{-}Q61K}$ OS 100 nM, and PC9 (EV). Osimertinib-preselected cells were cultured for 0, 7, and 21 days without osimertinib treatment and plated 48 h before lysis. **c** Cell viability assay of PC9 cells expressing the annotated constructs treated for 72 h with osimertinib is shown. The relative AUC (see Methods) of BRAF^{V600E} OS 100 nM and NRAS^{Q61K} OS 100 nM after osimertinib withdrawal for >40 days are shown. **d** Clonogenicity assay of PC9 cells expressing the annotated constructs treated for 14 days with indicated compounds before staining. **e** RNA-seq based expression of E2F gene set genes (rows) in PC9 derived cell lines (columns) after 48 h treatment with indicated inhibitors. Expression was normalized as *z*-score per gene. **f** Synergy screen of osimertinib and trametinib combination treatment in PC9 derived cell lines for 72 h are displayed. **g** Immunoblotting of PC9 cells expressing the annotated constructs is shown. Treatment with indicated compounds 48 h before lysis. **h** Relative tumor volume of xenograft mice injected with PC9$^{BRAF\text{-}V600E}$ OS 100 nM cells in % compared to day 0 of the treatment regimen (see Methods). Error bars indicate mean ± SD. Two-tailed paired *t* tests (all except (**h**); two-tailed Welch's *t* tests with Bonferonni-correction), $^{***}p < 0.001$, $^{**}p < 0.01$, $^{*}p < 0.05$, $^{n.s.}p > 0.05$. *EGFR* epidermal growth factor receptor, *BRAF* B-rapidly accelerated fibrosarcoma, *NRAS* neuroblastoma rat sarcoma, EV empty vector.

combination of dabrafenib plus trametinib (initiated at detection of *BRAF*^{V600E} mutation) was driven by an evolutionary branching process rather than a linear trajectory of one clone that continues to acquire additional resistance mutations. Moreover, in both patients, the different metastases are genetically distinct from each other but arise from common ancestors that do not carry a resistance mutation. Even within our limited cohort, we observe different patterns of clonal evolution: while for P04 a common ancestor most likely from the primary tumor gave rise to the different metastases, for patient P01 phylogenetic analyses are in accordance with a model supporting much earlier branching. Of note, resistance mutations such as *EGFR*^{T790M} and *BRAF*^{V600E} were not detected by either panel sequencing or WES in samples still sensitive to the respective inhibitors. This may indicate that they developed either de novo during treatment or were pre-existent, but at a frequency to low to be detected without selection pressure.

Overall, our results demonstrate the presence and further development of tumor heterogeneity that can give rise to multiple resistance mechanisms due to treatment selection pressure. Moreover, our genomic analysis emphasizes that we are faced with a complex mutational landscape based on intra-tumoral, inter-tumoral, and inter-patient heterogeneity. It thus constitutes a major clinical challenge for the development of an efficient treatment strategy to counteract tumor progression. Based on the present findings a diagnostic strategy aiming to address the multilayered heterogeneity e.g. using liquid biopsies or multiple re-biopsies appears warranted to optimize treatment schedules. Our data suggest that one promising treatment strategy for patients with concurrent *EGFR* and MAPK pathway activation may require alternating treatment regimens with intermittent changes between drug combinations based upon observed heterogenic tumor response and emerging resistance patterns. To facilitate this strategy FDG-PET can be quite useful for rapid treatment evaluation and hence, dynamic clinical management as demonstrated by our investigational approach. However, we are aware that more patients need to be profiled in the future to compliment our results.

We and others have previously found that acquired resistance through activation of MAPK signaling via *KRAS* mutations can be detected in patients receiving third-generation EGFR inhibitors[11,12]. *BRAF* mutations and *BRAF* rearrangements have also been shown to play a similar role like *KRAS* in the resistance setting of *EGFR*-mutant adenocarcinoma[16,19,34]. This is surprising as previous functional analyses indicated that mutant *KRAS* mutations may augment the cell death rate of *EGFR*-mutant cells and thereby limit the outgrowth of resistant clones[29]. Our cell line models indicate that concomitant MAPK pathway signaling is tolerated when *BRAF* or *NRAS* are activated. This corresponds with our clinical observation that *BRAF* mutations can co-occur with *EGFR* mutations even before anti-EGFR therapy. Interestingly, the levels of phospho-ERK activation differ strongly between *BRAF*- and *NRAS*-mutant cells but we did not observe major differences in the ability of these alleles to promote resistance or cell death in *EGFR*-mutant cells. These functional observations are also in line with our finding that *BRAF*/*EGFR*-mutant lung tumors are recurrently found across different cancer centers, indicating a basis for the co-existence of *BRAF*/*EGFR* mutations without selection pressure. Future studies are required to fully decipher the potential differences between MAPK signaling activation at different levels of the pathway in the context of *EGFR*-mutant lung adenocarcinoma. Nevertheless, our in vitro and in vivo findings fully support the notion that EGFR/MEK combination might be a viable option to overcome *BRAF*-driven resistance in patients with *EGFR*-mutant lung adenocarcinoma.

In summary, our data uncover basic principles of drug-induced evolutionary paths underlying *BRAF*-driven resistance in patients with lung adenocarcinoma. The integrated analyses support a model in which concomitant activation of EGFR and BRAF is selected through anti-EGFR therapy that combines well with EGFR, BRAF, and MEK inhibitors to overcome resistance. Our systematic exploration of clinically relevant drug combinations may offer additional avenues for follow-up investigations into novel targeted treatment strategies for patients with co-occurring *EGFR* and *BRAF* mutations.

METHODS

Patients

We compiled a cohort of 15 patients with lung adenocarcinoma and activating *EGFR* mutations that harbored co-occurring *BRAF* mutations with and without prior anti-EGFR treatment. Patients were identified within the Network Genomic Medicine (NGM) Lung Cancer in Cologne, Germany, Institute Gustave Roussy in Paris, France, and Cantonal Hospital of Lucerne, Switzerland. Treatment, genetic findings, and survival of these patients were evaluated. All patients consented to be analyzed. The study was conducted in concordance with local ethical guidelines and was reviewed by the institutional ethics committee. Selected patients were treated with different lines of therapy including combinations of osimertinib, dabrafenib, and trametinib. These patients provided written informed consent for a prospective investigational molecular- and imaging-guided personalized treatment approach. Rebiopsies were acquired at disease progression. Tissue biopsy was performed through core needle biopsy according to local standard procedures. Survival of all patients was calculated using the Kaplan Meier method.

Molecular analyses

The vast majority of the specimens analyzed in our study consisted of tumor tissue ($n = 13$). For two patients, liquid biopsies were evaluated. (Table 1). Next-generation sequencing (NGS)-based molecular profiling was performed for each patient either on tumor tissue or on circulating tumor DNA (ctDNA). For patients, P01 and P04 whole-exome sequencing was additionally performed on the tumor tissue. For patients P01 and P04, we obtained longitudinally serial repeated tissue biopsies of the leading tumor lesions at each time of progression during treatment with different combinations of osimertinib, dabrafenib and trametinib, and other therapies. NGS of tumor tissue was performed as previously described[35–38]. Plasma analysis of ctDNA was performed as previously reported[39].

PET-CT assessments

The efficacy of treatment was evaluated by positron emission tomography (PET)/computed tomography (CT) scans using radiolabeled ^{18}F-2-fluoro-2-deoxy-D-glucose (FDG). Scans were acquired at baseline, and as early as 2 weeks (early assessment) and again at regular intervals roughly every 6 or more weeks (late assessments) after initiation or change of therapy to capture early metabolic response (measured by standard uptake value (SUV)max) and morphologic response over time. Scans were conducted as previously described and performed on a Biograph mCT Flow-Edge 128 PET/CT-system (Siemens Medical Solutions) with a 128-slice spiral CT component from the base of the skull to the mid-thigh[40]. We followed Positron Emission Response Criteria in Solid Tumors version 1.0 guidelines, assuming that response is characterized by an SUV reduction of at least 30% in the hottest lesion[41].

Whole-exome sequencing (WES)

WES was performed on FFPE-derived DNA from serial tumor tissue rebiopsies obtained at the time of tumor progression during treatment of patients P01 and P04. In addition, for one patient DNA was extracted from the primary tumor using the truXTRAC FFPE DNA extraction kit (Covaris, USA, Cat. No. 520307). Exomes were individually prepared using 200 ng of DNA using standard protocol SureSelectXT Automated Target Enrichment for Illumina Paired-End Multiplexed Sequencing and Agilent Bravo automated liquid handling platform. As for patient P14, there was only a post-osimertinib tumor biopsy available for WES, which was enriched using the Agilent SureSelect CR kit (Agilent, USA). After validation (2200 TapeStation, Agilent Technologies) and quantification (Qubit System, Invitrogen, Waltham, USA) pools of libraries were generated. The pools were quantified using the KAPA Library Quantification kit (Peqlab, Germany, KAPBKK4854) and 7900HT Sequence Detection System (Applied Biosystems, Waltham, USA) and subsequently sequenced at 140× mean coverage on an Illumina NovaSeq6000 sequencing instrument using a paired-end 2 × 100 bp protocol.

WES and clonality analysis

Analysis of raw sequencing data and clonality analyses were performed using an established pipeline[42]: After alignment of the raw sequencing data to the hg19 reference genome in total 137–325 million reads could successfully be mapped per sample corresponding to a mean coverage of 93×–200× per sample and covering all intended exonic target region with ≥20× coverage for 90–98% of those. In summary, of the 42.3 megabases of exonic regions as defined by the GRCh 37/hg19 RefSeq genome annotation, 39–40 megabases of exons were sufficiently covered for mutation calling and subsequent analyses. Thus, allelic fractions of somatic mutations were corrected for purity and CN changes to determine cancer cell fractions (CCF). The distribution of CCFs was then searched for distinct subpopulations by using a nonparametric method to deconvolute the noise in the CCFs. This allows for the identification of genetically distinct tumor subclones and the reconstruction of tumor evolutionary histories.

Cell culture and functional analyses

Human NSCLC cell lines were verified by STR profiling at the Institute for Forensic Medicine of the University Hospital of Cologne. PC9, HCC827, and HEK293T cell lines were obtained from ATCC. PC9 and HCC827 cells and their osimertinib-preselected derivatives were cultured in RPMI (Fisher Scientific, USA, Cat. No. 12004997) HEK293T cells were cultured in DMEM (Fisher Scientific, USA, Cat. No. 61965-026). All media were supplemented with 10% fetal bovine serum (Fisher Scientific, USA, Cat. No. 10270-106) and 1% penicillin/streptomycin (Fisher Scientific, USA, Cat. No. 15070-063). All cells were grown at 37 °C in a humidified atmosphere with 5% CO_2.

Reagents

For cell culture studies, osimertinib (LC Laboratories, USA, Cat. No. 1421373-65-0), trametinib (LC Laboratories, USA, Cat. No. 871700-17-3), and vemurafenib (LC Laboratories, USA, Cat. No. 918504-65-1) were dissolved in dimethyl sulfoxide (DMSO) (Carl Roth, Germany, Cat. No. 4720.4) to a final stock concentration of 10 mM. Cisplatin (pharmacy of University Hospital of Cologne) was diluted to 3.33 mM in 0.9% NaCl.

Crystal violet assay

Totally, 10^5 cells were plated into one well of a 6-well plate and treated with DMSO (control), 300 nM osimertinib, 100 nM trametinib, 1 µM vemurafenib, and combinations osimertinib plus trametinib and osimertinib plus vemurafenib. Seven or 14 days after treatment, cells were fixed in 4% paraformaldehyde (Carl Roth, Germany, Cat. No. CP10.1) in phosphate-buffered saline (PBS) (Fisher Scientific, USA, Cat. No. 14190144), stained with 0.1% crystal violet (Sigma Aldrich, USA, Cat. No. C3886-25G) in PBS, and rinsed in PBS before image acquisition. For quantification, the Crystal Violet dye was dissolved in 2 ml methanol (Carl Roth, Germany, Cat. No. CP43.4) in the 6-well plate. Twenty microlitres of this solution were diluted 1:10 with methanol and injected into 96-well plates. The read-out was the absorption at 560 nm wavelength. The results per cell line were normalized against their DMSO-controls and then against the empty vector (EV) control cell line.

Protein overexpression experiments

Vectors pBABE puro, pBABE-puro-BRAF^{V600E}, and pBABE-NRAS^{Q61K} were cotransfected with a helper plasmid into HEK 293T cells using TransIT-LT1 reagent (Mirus, USA, Cat. No. MIR2300). Forty-eight hour post transfection, replication-incompetent retroviruses were collected from the supernatant for infection of PC9 and HCC827 in the presence of 8 µg/ml polybrene (Merck Millipore, USA, Cat. No. TR1003-G). Twenty-four hour after infection, the growth medium was changed and 3 µg/ml (PC9) or 2 µg/ml (HCC827) puromycin (Sigma Aldrich, USA, Cat. No. p8833) was added for selection for 7 days. After selection, cells were analyzed for protein expression.

pBABE-puro was a gift from Hartmut Land & Jay Morgenstern & Bob Weinberg (Addgene plasmid # 1764; RRID:Addgene_1764).

pBabe-Puro-BRAF^{V600E} was a gift from William Hahn (Addgene plasmid # 15269; RRID:Addgene_15269).

pBabe-NRAS^{Q61K} was a gift from Channing Der (Addgene plasmid # 12543; RRID:Addgene_12543).

Cell viability screening

To assess cell viability, cells were plated in 96-well plates in triplicates, and compounds were added at 9 decreasing compound concentrations 24 h after seeding. Seventy-two hours later, cell viability was measured via Cell Titer-Glo (CTG) assay (Promega, USA, Cat. No. g7573) and was normalized to DMSO-treated controls. Resistance in % was calculated as the area under the curve (AUC), calculated via Gauss's trapezoid area formula and then divided by a theoretical non-responding AUC, all calculated in R. Data are represented as mean ± standard error of the mean and significance was calculated by paired Student's *t* tests.

RNA isolation and qRT-PCR

Totally, 5×10^5 cells were plated into one well of a 6-well plate and harvested after 24 h. Total RNA was isolated using the RNeasy-kit (Qiagen, Germany, Cat. No. 74106) according to the manufacturer's instructions, including DNAse I digestion (Qiagen, Germany, Cat. No. 79256). In all, 1.5 µg of total RNA was reverse transcribed using Super-script II (Thermo Fisher Scientific, USA, Cat. No. 18064022) with random hexamer primers. Quantitative real-time PCR (qPCR) was performed using the QuantStudio 3 Real-Time PCR System (Thermo Fisher Scientific) and Power SYBR Green PCR Master Mix (Thermo Fisher Scientific, USA, Cat. No. 4309155). Data were normalized to GAPDH RNA levels and are presented as mean ± SD and significance was calculated by paired Student's *t* tests.

Flow cytometry

Cell lines were seeded into 6-well plates (1×10^5 cells/well). Twenty-four-hour later Staurosporine (Sigma Aldrich, USA, S4400) or DMSO control was added to the medium. Twenty-four-hour later supernatant was collected, cells were trypsinized (Fisher Scientific, USA, Cat. No. 11560626), washed with ice-cold PBS, and resuspended in antibody-binding buffer (10 mM HEPES pH 7.4 (Fisher Scientific, USA, Cat. No. 15630080), 140 mM NaCl; 2.5 mM $CaCl_2$). Cells were stained for Annexin-V (BD Biosciences, USA, Cat. No. 556420) and 50 µg/mL propidium iodide (Carl Roth, Germany, Cat. No. CN74). After 20 min of incubation in the dark, samples were analyzed on a FACS Gallios Flow Cytometer (Beckman Coulter). We used FACS Kaluza software (Beckman Coulter) to quantify populations. At least 5×10^4 events were assessed per measurement. All measurements were performed as duplicates. Gates used can be found in Supplementary Fig. 8. Data are presented as mean ± SD.

Immunoblot

Cell lysates were prepared using RIPA buffer supplemented with protease inhibitors (Complete Mini Protease Inhibitor Cocktail, Roche, Switzerland, Cat. No. 11836170001). Protein concentration was determined by BCA assay (Thermo Fisher Scientific, USA, Cat. No. 23225) and equal amounts of protein (20 µg) were separated on 4–12% Tris-glycine sodium dodecyl sulfate-polyacrylamide gel electrophoresis gels (Thermo Fisher Scientific, USA, Cat. No. XP04125BOX) and transferred to PVDF-FL membrane (Sigma Aldrich, USA, Cat. No. IPFL00010). Membranes were blocked in 5% milk (Carl Roth, Germany, Cat. No. T145.1) blocking buffer in Tris-buffered saline (TBS), incubated with primary antibodies, washed, and incubated with fluorescently labeled secondary antibodies before detection with Odyssey CLx imaging system (LI-COR Biosciences). Images were processed using the Image Studio Software (LI-COR Biosciences). Primary antibodies are EGFR (Cell Signaling, USA, Cat. No. CS-4267), p-EGFR (Cell Signaling, USA, Cat. No. CS-3777), BRAF-V600E (Spring Bioscience, USA, Cat. No. E-19290), BRAF (Santa Cruz Biotechnology, USA, Cat. No. SC-5284), ERK (Cell Signaling, USA, Cat. No. CS-9102), p-ERK (Cell Signaling, USA, Cat. No. CS-4370), Akt (Cell Signaling, USA, Cat. No. CS-2920), p-Akt (Cell Signaling, USA, Cat. No. CS-9271) and Hsp90 (Cell Signaling, USA, Cat. No. CS-4877). All primary antibodies were diluted 1:1000 in 5% milk blocking buffer in TBS with 0.2% Tween®20 (Sigma Aldrich, USA, Cat. No. P7949-500ML). Secondary antibodies are goat anti-rabbit 800CW (LI-COR Biosciences, USA, Cat. No. 926-32211), goat anti-mouse 800CW (LI-COR Biosciences, USA, Cat. No. 926-3220), goat anti-rabbit 680LT (LI-COR Biosciences, USA, Cat. No. #926-68021), and goat anti-mouse 680LT (LI-COR Biosciences, USA, Cat. No. 926-68020). All secondary antibodies were diluted 1:20,000 in 2.5% milk blocking buffer in TBS with 0.2% Tween®20 and 0.01% sodium dodecyl sulfate (SDS) (Carl Roth, Germany, Cat. No. 8029.4).

All blots derive from the same experiment and were processed in parallel. Uncropped blots can be found in Supplementary Figs. 9–13.

Synergy screen

Cells were plated in a 6×6 wells matrix in 96-well plates. After 24 h cells were treated with five decreasing concentrations of compound A plus DMSO control starting from right to left. Cells were also treated at the same time with five decreasing concentrations of compound B plus DMSO control starting from the bottom to the top. The topmost left well is only treated with DMSO, while the bottommost right well is treated with the highest concentration of both compounds. The following starting concentrations were used: 300 nM of osimertinib, 100 nM of trametinib, and 1 µM of vemurafenib. Seventy-two hours after treatment, cell viability was measured via CTG assay and was normalized to DMSO-treated controls. Synergy scores were then calculated in R using the SynergyFinder Package and the Zero Interaction Potency (ZIP) reference model as implemented in the package. The mean of the nine highest synergy scores from each matrix is presented ±SD and significance were calculated by paired Student's *t* tests.

3D Synergy screen

Cells were plated as described in "Synergy screen", just on six plates, each with a set concentration of vemurafenib to add a third dimension. Cells were treated for the same time and with the same concentration as in "Synergy screen". Cell viability was measured the same way as in "Synergy screen". The expected drug combination responses were calculated based on ZIP reference model using SynergyFinder[43]. Deviations between observed and expected responses with positive and negative values denote synergy and antagonism, respectively.

Growth series

Totally, 1×10^5 cells per well were plated 5 times in triplicates per cell line in 6-well plates. For 5 days, always after 24 h, one triplicate of each cell line was trypsinized and counted via Z Series Coulter Counter (Beckmann Coulter). Results were normalized to day 1 and were anticipated from the slope of a best-fitting line through each data set Data are presented as mean ± SD.

Generating osimertinib selected cell lines

$PC9^{BRAF\text{-}V600E}$, $PC9^{NRAS\text{-}Q61K}$, and $HCC827^{BRAF\text{-}V600E}$ cell lines were each treated with 10 nM or 100 nM osimertinib respectively for >30 days. After that cells were labeled osimertinib selected (OS) 10 nM or 100 nM, respectively, and experiments were performed. Even after >30 days osimertinib treatment in cell culture, cells were continuously kept under osimertinib treatment.

3′UTR-RNA sequencing

For each cell line (PC9 pBABE EV, PC9 pBABE $BRAF^{V600E}$, and PC9 pBABE $BRAF^{V600E}$ OS 100) 5×10^5 cells were plated and left to adhere overnight. The next day they were treated with 300 nM osimertinib, 100 nM trametinib, a combination of both, or DMSO control for 48 h. RNA extraction and sequencing were performed using the Qiagen RNeasy Mini kit following the manufacturer's instruction. Totally, 500 ng total RNA were used to prepare 3′ UTR mRNA libraries using the Lexogen QuantSeq kit (Lexogen, Austria, Cat. No. 015.96) according to the standard protocol[44]. Quality controlled cDNA pools were quantified with the KAPA Library Quantification kit and sequenced on a NovaSeq sequencer (Illumina, USA) with a 1×100 bp protocol. Raw data were aligned to the human genome reference GRCh38 using STAR aligner[45] and gene expression was quantified with RSEM[46] prior to downstream analysis with the R package DESeq2[47]. E2F target genes were obtained from the MSigDB Hallmark collection and MAPK feedback genes from a recently published MAPK activity score[31].

In vivo xenograft model

The local authorities and the animal protection committee approved all animal procedures of this study.

$PC9^{BRAF\text{-}V600E}$ OS100 nM cells (5×10^6) were resuspended in 100 µL PBS and then inoculated subcutaneously in both flanks of 8- to 12-week-old female nude mice (RJ:NMRI-FOXN1 NU, Janvier Labs) and treatment was initiated when tumors reached a mean volume of approximately 50 mm^3. Mice were treated daily for 21 days orally with vehicle solution (1% DMSO, 30% PEG300, 0.5% hydroxypropyl methylcellulose, 0.2% Tween-80, ddH_2O) QD, osimertinib (5 mg/kg in 1% DMSO + 30% PEG300 + ddH_2O) QD, trametinib (1 mg/kg in 0.5% hydroxypropyl methylcellulose, 0.2% Tween-80, ddH_2O) QD or combination (osimertinib as described before and trametinib as described before) Tumor volumes were measured daily in two dimensions using a caliper, and the volume was expressed in mm^3 using the formula: $V = 0.5 \times (\text{length} \times \text{width}^2)$, where V is tumor volume, length is the longest tumor dimension and width is the longest tumor dimension perpendicular to the length.

Reporting summary

Further information on research design is available in the Nature Research Reporting Summary linked to this article.

DATA AVAILABILITY

The data generated and analyzed during this study are described in the manuscript and Supplementary Material. WES data were uploaded to The European Genome-phenome Archive (EGA) with the accession code EGAS00001005614. RNA sequencing data were uploaded to ArrayExpress with the accession code E-MTAB-11004. All relevant data and materials that support the findings of this work are available from the corresponding authors upon reasonable request.

CODE AVAILABILITY

No custom code or algorithms were created.

Received: 25 February 2021; Accepted: 16 November 2021;
Published online: 17 December 2021

REFERENCES

1. Skoulidis, F. & Heymach, J. V. Co-occurring genomic alterations in non-small-cell lung cancer biology and therapy. *Nat. Rev. Cancer* **19**, 495–509 (2019).
2. Mok, T. S. et al. Gefitinib or carboplatin–paclitaxel in pulmonary adenocarcinoma. *N. Engl. J. Med.* **361**, 947–957 (2009).
3. Rosell, R. et al. Erlotinib versus standard chemotherapy as first-line treatment for European patients with advanced EGFR mutation-positive non-small-cell lung cancer (EURTAC): a multicentre, open-label, randomised phase 3 trial. *Lancet Oncol.* **13**, 239–246 (2012).
4. Sequist, L. V. et al. Phase III study of afatinib or cisplatin plus pemetrexed in patients with metastatic lung adenocarcinoma with EGFR mutations. *J. Clin. Oncol.* **31**, 3327–3334 (2013).
5. Wu, Y.-L. et al. Dacomitinib versus gefitinib as first-line treatment for patients with EGFR-mutation-positive non-small-cell lung cancer (ARCHER 1050): a randomised, open-label, phase 3 trial. *Lancet Oncol.* **18**, 1454–1466 (2017).

6. Cross, D. A. E. et al. AZD9291, an irreversible EGFR TKI, overcomes T790M-mediated resistance to EGFR inhibitors in lung cancer. *Cancer Discov.* **4**, 1046–1061 (2014).
7. Jänne, P. A. et al. AZD9291 in EGFR inhibitor-resistant non-small-cell lung cancer. *N. Engl. J. Med.* **372**, 1689–1699 (2015).
8. Soria, J.-C. et al. Osimertinib in untreated EGFR-mutated advanced non-small-cell lung cancer. *N. Engl. J. Med.* **378**, 113–125 (2018).
9. Ramalingam, S. S. et al. Overall survival with osimertinib in untreated, EGFR-mutated advanced NSCLC. *N. Engl. J. Med* https://doi.org/10.1056/nejmoa1913662 (2019).
10. Leonetti, A. et al. Resistance mechanisms to osimertinib in EGFR-mutated non-small cell lung cancer. *Br. J. Cancer* **121**, 725–737 (2019).
11. Ortiz-Cuaran, S. et al. Heterogeneous mechanisms of primary and acquired resistance to third-generation EGFR inhibitors. *Clin. Cancer Res.* https://doi.org/10.1158/1078-0432.ccr-15-1915 (2016).
12. Michels, S. et al. Genomic profiling identifies outcome-relevant mechanisms of innate and acquired resistance to third-generation epidermal growth factor receptor tyrosine kinase inhibitor therapy in lung cancer. *JCO Precis. Oncol.* https://doi.org/10.1200/po.18.00210 (2019).
13. Tumbrink, H. L., Heimsoeth, A. & Sos, M. L. The next tier of EGFR resistance mutations in lung cancer. *Oncogene* https://doi.org/10.1038/s41388-020-01510-w (2020).
14. Thress, K. S. et al. Acquired EGFR C797S mutation mediates resistance to AZD9291 in non-small cell lung cancer harboring EGFR T790M. *Nat. Med.* https://doi.org/10.1038/nm.3854 (2015).
15. Chabon, J. J. et al. Circulating tumour DNA profiling reveals heterogeneity of EGFR inhibitor resistance mechanisms in lung cancer patients. *Nat. Commun.* **7**, 11815 (2016).
16. Eberlein, C. A. et al. Acquired resistance to mutant-selective EGFR inhibitor AZD9291 is associated with increased dependence on RAS signaling in preclinical models. *Cancer Res.* https://doi.org/10.1158/0008-5472.can-14-3167 (2015).
17. Ricordel, C., Friboulet, L., Facchinetti, F. & Soria, J.-C. Molecular mechanisms of acquired resistance to third-generation EGFR-TKIs in EGFR T790M-mutant lung cancer. *Ann. Oncol.* **29**, i28–i37 (2018).
18. Fassunke, J. et al. Overcoming EGFRG724S-mediated osimertinib resistance through unique binding characteristics of second-generation EGFR inhibitors. *Nat. Commun.* **9**, 4655 (2018).
19. Ohashi, K. et al. Lung cancers with acquired resistance to EGFR inhibitors occasionally harbor BRAF gene mutations but lack mutations in KRAS, NRAS, or MEK1. *Proc. Natl Acad. Sci. USA* **109**, E2127–E2133 (2012).
20. Ho, C.-C. et al. Acquired BRAF V600E mutation as resistant mechanism after treatment with osimertinib. *J. Thorac. Oncol.* **12**, 567–572 (2017).
21. Bracht, J. W. P. et al. BRAF mutations classes I, II, and III in NSCLC patients included in the SLLIP trial: the need for a new pre-clinical treatment rationale. *Cancers* **11**, 1381 (2019).
22. Planchard, D. et al. Dabrafenib plus trametinib in patients with previously treated BRAF(V600E)-mutant metastatic non-small cell lung cancer: an open-label, multicentre phase 2 trial. *Lancet Oncol.* **17**, 984–993 (2016).
23. Planchard, D. et al. Dabrafenib plus trametinib in patients with previously untreated BRAFV600E-mutant metastatic non-small-cell lung cancer: an open-label, phase 2 trial. *Lancet Oncol.* **18**, 1307–1316 (2017).
24. Ding, H. et al. Durable clinical response of advanced lung adenocarcinoma harboring EGFR-19del/T790M/BRAF^{V600E} mutations after treating with osimertinib and dabrafenib plus trametinib: a case report. *Oncotargets Ther.* **ume 13**, 7933–7939 (2020).
25. Huang, Y., Gan, J., Guo, K., Deng, Y. & Fang, W. Acquired BRAF V600E mutation mediated resistance to osimertinib and responded to osimertinib, dabrafenib, and trametinib combination therapy. *J. Thorac. Oncol.* **14**, e236–e237 (2019).
26. Meng, P. et al. Combined osimertinib, dabrafenib and trametinib treatment for advanced non-small-cell lung cancer patients with an osimertinib-induced BRAF V600E mutation. *Lung Cancer* **146**, 358–361 (2020).
27. Xie, Z. et al. Lung adenocarcinoma harboring concomitant EGFR mutations and BRAF V600E responds to a combination of osimertinib and vemurafenib to overcome osimertinib resistance. *Clin. Lung Cancer* https://doi.org/10.1016/j.cllc.2020.06.008 (2020).
28. Cun, Y., Yang, T.-P., Achter, V., Lang, U. & Peifer, M. Copy-number analysis and inference of subclonal populations in cancer genomes using Sclust. *Nat. Protoc.* **13**, 1488–1501 (2018).
29. Unni, A. M. et al. Hyperactivation of ERK by multiple mechanisms is toxic to RTK-RAS mutation-driven lung adenocarcinoma cells. *Elife* **7**, e33718 (2018).
30. McFadden, D. G. et al. Mutational landscape of EGFR-, MYC-, and Kras-driven genetically engineered mouse models of lung adenocarcinoma. *Proc. Natl Acad. Sci. USA* **113**, E6409–E6417 (2016).
31. Wagle, M.-C. et al. A transcriptional MAPK Pathway Activity Score (MPAS) is a clinically relevant biomarker in multiple cancer types. *Npj Precis. Oncol.* **2**, 7 (2018).
32. Poulikakos, P. I., Zhang, C., Bollag, G., Shokat, K. M. & Rosen, N. RAF inhibitors transactivate RAF dimers and ERK signalling in cells with wild-type BRAF. *Nature* **464**, 427–430 (2010).
33. Oxnard, G. R. et al. Assessment of resistance mechanisms and clinical implications in patients with EGFR T790M-positive lung cancer and acquired resistance to osimertinib. *JAMA Oncol.* **4**, 1527–1534 (2018).
34. Vojnic, M. et al. Acquired BRAF rearrangements induce secondary resistance to EGFR therapy in EGFR-mutated lung cancers. *J. Thorac. Oncol.* **14**, 802–815 (2019).
35. König, K. et al. Implementation of amplicon parallel sequencing leads to improvement of diagnosis and therapy of lung cancer patients. *J. Thorac. Oncol.* **10**, 1049–1057 (2015).
36. Peifer, M. et al. Integrative genome analyses identify key somatic driver mutations of small-cell lung cancer. *Nat. Genet* **44**, 1104–1110 (2012).
37. George, J. et al. Comprehensive genomic profiles of small cell lung cancer. *Nature* **524**, 47–53 (2015).
38. Recondo, G. et al. Feasibility and first reports of the MATCH-R repeated biopsy trial at Gustave Roussy. *Npj Precis. Oncol.* **4**, 27 (2020).
39. Remon, J. et al. Real-world utility of an amplicon-based next-generation sequencing liquid biopsy for broad molecular profiling in patients with advanced non–small-cell lung cancer. *JCO Precis. Oncol.* **3**, 1–14 (2019).
40. Kuhnert, G. et al. Impact of PET/CT image reconstruction methods and liver uptake normalization strategies on quantitative image analysis. *Eur. J. Nucl. Med. Mol. Imaging* **43**, 249–258 (2016).
41. Wahl, R. L., Jacene, H., Kasamon, Y. & Lodge, M. A. From RECIST to PERCIST: evolving considerations for PET response criteria in solid tumors. *J. Nucl. Med.* **50**, 122S–150S (2009).
42. Herling, C. D. et al. Clonal dynamics towards the development of venetoclax resistance in chronic lymphocytic leukemia. *Nat. Commun.* **9**, 727 (2018).
43. Ianevski, A., Giri, K. A. & Aittokallio, T. SynergyFinder 2.0: visual analytics of multi-drug combination synergies. *Nucleic Acids Res.* **48**, W488–W493 (2020).
44. Brägelmann, J. et al. Systematic kinase inhibitor profiling identifies CDK9 as a synthetic lethal target in NUT midline carcinoma. *Cell Rep.* **20**, 2833–2845 (2017).
45. Dobin, A. et al. STAR: ultrafast universal RNA-seq aligner. *Bioinformatics* **29**, 15–21 (2013).
46. Li, B. & Dewey, C. N. RSEM: accurate transcript quantification from RNA-Seq data with or without a reference genome. *BMC Bioinforma.* **12**, 323 (2011).
47. Love, M. I., Huber, W. & Anders, S. Moderated estimation of fold change and dispersion for RNA-seq data with DESeq2. *Genome Biol.* **15**, 550 (2014).

ACKNOWLEDGEMENTS

We thank all members of the Sos lab and Peifer lab for their fruitful comments, especially Katia Garbert. We furthermore thank the Regional Computing Center of the University of Cologne (RRZK) for providing computing time on the DFG-funded HPC cluster CHEOPS as well as support and Graziella Bosco for data archiving at EGA. This work was supported by the Bundesministerium für Bildung und Forschung [e:Med initiative; 01ZX1901A to M.L.S., M.P. and R.K.T.]; a research grant by the Thyssen Foundation [10.19.2.025MN to M.L.S.] and the Deutsche Krebshilfe [70112888 to M.L.S., Mildred Scheel Nachwuchszentrum Grant 70113307 to J.B. and D.F.A.]; and the Else Kröner Fresenius Stiftung [Memorial Grant 2018_EKMS.35 to J.B.]. The funding sources had no involvement in the conceptual or executive process of this study.

AUTHOR CONTRIBUTIONS

Each author confirms that he or she has made substantial contributions to the conception or design of the work or the acquisition, analysis, interpretation, and assembly of the data; contributed to paper writing; all authors approved the final paper; all authors are accountable for all aspects of the work. D.S. and D.F.A. contributed equally to this work as co-first authors. J.B., M.S., and M.L.S. contributed equally to this work as co-senior authors.

FUNDING

Open Access funding enabled and organized by Projekt DEAL.

COMPETING INTERESTS

D.S. has received honoraria for advisory roles or lectures from BMS, Boehringer-Ingelheim, MSD, Novartis, Roche, Healthcare Consulting Cologne, Abbvie; and has received travel and accommodation support from AstraZeneca, BMS, Boehringer-Ingelheim, MSD, Novartis, Roche, Abbvie. J.F. has received honoraria from AstraZeneca. B.B. has received sponsored research at Gustave Roussy Cancer Center from Abbvie, Amgen, AstraZeneca, BioGen, Blueprint Medicines, BMS, Boehringer Ingelheim, Celgene, Cristal Therapeutics, Daiichi-Sankyo, Eli Lilly, GSK, Ignyta, IPSEN,

Inivata, Janssen, Merck KGaA, MSD, Nektar, Onxeo, OSE immunotherapeutics, Pfizer, Pharma Mar, Roche-Genentech, Sanofi, Servier, Spectrum Pharmaceuticals, Takeda, Tiziana Pharma, Tolero Pharmaceuticals. D.P. has had consulting or advisory roles for AstraZeneca, BMS, Boehringer Ingelheim, Celgene, Daiichi Sankyo, Eli Lilly, Merck, Novartis, Pfizer, prIME Oncology, Peer CME, Roche, Samsung Bioepis; and has received honoraria from AstraZeneca, BMS, Boehringer Ingelheim, Celgene, Eli Lilly, Merck, Novartis, Pfizer, prIME Oncology, Peer CME, Roche, Samsung Bioepis; and has done clinical trials research as principal or co-investigator (institutional financial interests) with support from AstraZeneca, BMS, Boehringer Ingelheim, Eli Lilly, Merck, Novartis, Pfizer, Roche, Medimmun, Sanofi-Aventis, Taiho Pharma, Novocure, Inivata, Takeda, Pharma Mar, Janssen, Daiichi Sankyo; and has received travel and accommodation support from AstraZeneca, Roche, Novartis, Pfizer. L.N. has received honoraria from Pfizer, Celgene, Novartis, Roche, Boehringer Ingelheim, Janssen, BMS, Takeda, Bayer; and has had consulting or advisory roles for Novartis, Boehringer Ingelheim, BMS, Roche, Janssen, Pfizer, Takeda, Bayer; and has received research funding from Pfizer, Novartis, MSD, Janssen, Amgen; and has received travel and accommodation support from Novartis, Pfizer, Celgene, Boehringer Ingelheim, Janssen. S.M. has received honoraria from Pfizer, Novartis, AstraZeneca; and has received research support from Novartis, Pfizer, BMS, Janssen. R.K.T. is the founder/shareholder and has had a consultancy/advisory role of/for PearlRiver Bio GmbH; is the founder/shareholder and has had a consultancy/advisory role of/for Epiphanes Inc; and is the founder/shareholder and has had a consultancy/advisory role of/for CDL Therapeutics GmbH; and has a stock or other ownership and has had a consultancy/advisory role of/for Merck, J&J, AstraZeneca, Bayer; and has a stock or other ownership and has had a consultancy/advisory role of/for Roche; and has a commercial research grant from Roche; and has a stock or other ownership of Novartis, GSK; and has had a consultancy/advisory role for New Oncology AG, Clovis, Daiichi-Sankyo, Boehringer Ingelheim, MSD, Lilly, Sanofi-Aventis, Puma. S.M.-B. has received honoraria for advisory boards or lectures from BMS, Novartis, Roche, Pfizer, Bayer, Molecular Health, Targos, Astra Zeneca; and has received non-financial support from BMS, Janssen. O.G. has received honoraria for advisory boards from AMGEN, LILLY, BAYER. L.M. has had consulting or advisory roles for Roche Diagnostics, Takeda, Roche; and has had a lecture or educational activities for BMS, Tecnofarma, Roche; and has received travel and accommodation support from BMS, Roche; and has received Mentorship program with key opinion leaders from AstraZeneca; and has received sponsored research from Amgen, BMS, Boehringer Ingelheim. T.W. has had an advisory role for Lilly; and has received speakers honoraria from Novartis; and has received travel support from Roche, Pfizer. R.B. is co-founder and chief scientific officer of Targos Mol Inc., Kassel Germany; and has received personal fees and others for advisory boards or lectures from BMS, MSD, Novartis, Roche, Lilly, AstraZeneca, Illumina, AbbVie, Amgen, Boehringer-Ingelheim, Merk-Serono, Qiagen, Pfizer. J.W. has received honoraria for advisory roles or lectures from Amgen, AstraZeneca, Blueprint, BMS, Boehringer Ingelheim, Chugai, Daiichi Sankyo, Ignyta, Janssen, Lilly, Loxo, MSD, Novartis, Pfizer, Roche, Seattle Genetics, Takeda; and has received research support from BMS, Janssen Pharmaceutica, Novartis, Pfizer. M.S. has received honoraria for advisory roles from Pfizer, Roche, AMGEN, Novartis, Takeda, Boehringer Ingelheim; and has received institutional research support from AMGEN, Dracen Pharmaceuticals. M.L.S. is a founder, shareholder and advisor of PearlRiver Bio – a Centessa Pharmaceuticals company - and MLS has a commercial research grant from PearlRiver Bio - a Centessa company. The remaining authors declare no competing interests.

ADDITIONAL INFORMATION

Supplementary information The online version contains supplementary material available at https://doi.org/10.1038/s41698-021-00241-9.

Correspondence and requests for materials should be addressed to Johannes Brägelmann, Matthias Scheffler or Martin L. Sos.

Reprints and permission information is available at http://www.nature.com/reprints

Publisher's note Springer Nature remains neutral with regard to jurisdictional claims in published maps and institutional affiliations.

4. Discussion

This study addresses resistance mechanisms in *EGFR*-mutated LUAD, with a specific focus on the emergence and functional implications of co-expressed *BRAF* mutations. Driven by the initial hypothesis that co-activation of $EGFR^{del19}$ and $BRAF^{V600E}$ might result in synthetic lethality, the project employed genetically engineered cell models, in vivo xenografts, and patient cohort analyses to investigate this phenomenon. In contrast to the initial hypothesis, co-expression of $EGFR^{del19}$ and $BRAF^{V600E}$ promoted resistance to EGFR inhibition via reactivation of MAPK signalling rather than inducing cell death. The concomitant occurrence of *EGFR* and *BRAF* mutations was identified in five patients from the patient cohort at the time of initial diagnosis and in 10 patients as a resistance mechanism to EGFR-TKI therapy[54]. Using patient-derived NSCLC cell lines harbouring $EGFR^{del19}$ and $BRAF^{V600E}$ mutations, it was demonstrated that dual inhibition of EGFR and MEK by osimertinib and trametinib, respectively, overcomes resistance in *in vitro* experiments and in *in vivo* xenograft models.

4.1 Strengths and limitations

A particular strength of this work is the use of complementary experimental systems, enabling functional investigation as well as translational validation. The employment of isogenic cell line models provided controlled conditions to explain the biological consequences of $BRAF^{V600E}$ expression in *EGFR*-mutated backgrounds. *In vivo* xenograft experiments further confirmed the therapeutic potential of combined EGFR and MEK inhibition. Patient-derived genomic data add clinical relevance by illustrating the clonal emergence of *BRAF* mutations under *EGFR*-targeted treatment pressure. The clinical relevance of *BRAF* mutations as resistance mechanisms to EGFR-TKIs is increasingly recognized, yet functional data characterizing the co-occurrence of these mutations has been limited. This work fills an important gap by providing mechanistic validation and highlighting MAPK pathway reactivation as a critical driver of resistance in TKI-treated EGFR-mutated LUAD.

Limitations of this study include the use of engineered cell models that do not reflect the heterogeneity and complexity of the tumour microenvironment and impacts of the immune system. The patient cohort analysed comprised only 15 patients and was analysed retrospectively, which may limit the generalizability of the findings. Investigating non-genomic resistance mechanisms, immunogenic response and microenvironmental factors represent important future areas of research.

4.2 Research question

Earlier studies have established the principle that concurrent *EGFR* and *KRAS* mutations are mutually exclusive due to toxic ERK hyperactivation[1,2]. Correspondingly, mechanistic models have proposed the concept of an “oncogene overdose,” in which excessive ERK pathway activation surpasses a critical signaling threshold and leads to cytotoxicity or growth arrest[1,3,55].

Building on this, the present work tested a similar paradigm for BRAF in the context of *EGFR*-mutant LUAD, given its role downstream of RAS in the MAPK cascade. In our study, *BRAF*^{V600E} expression in *EGFR*-mutant NSCLC cells resulted in MAPK pathway reactivation and resistance to EGFR inhibition without triggering apoptotic cell death[54]. These findings suggest that *BRAF*^{V600E}-induced ERK signaling does not exceed the toxic signaling thresholds observed with KRAS. Noteworthy, mRNA expression of *BRAF*^{V600E} could be significantly increased in the polyclonal pool of cells through long-term selection with osimertinib[54]. Whether *BRAF*^{V600E} expression could be increased on a single-cell basis or whether cells with increased *BRAF*^{V600E} expression were selected out in advance cannot be determined with this experiment design and requires further investigation. Within this study context, concurrent *EGFR* and *BRAF* mutations had no cellular fitness disadvantages but also no growth advantages without simultaneous inhibition of EGFR. One possible reason for stronger p-ERK signalling in the case of concurrent *EGFR* and *KRAS* mutations rather than *EGFR* and *BRAF* co-mutation is the position of KRAS directly upstream of RAF, which might augment signal transduction. Whereas BRAF predominantly activates the MAPK-cascade via MEK and ERK, [56] KRAS signalling into the PI3K-AKT-mTOR-pathway could lead to the possibility that cell toxicity may be caused by pathways other than the MAPK pathway. However, Unni et al. demonstrated that synthetic lethality was mediated by ERK hyperactivation and AKT activation that was not rescued by using a PI3K-inhibitor, which had no effect on cell toxicity[2]. In summary, our functional preclinical data, as well as the data from patients with *BRAF* and *EGFR* mutations before receiving EGFR-TKI therapy, showed that *BRAF* mutations in the context of an *EGFR* mutation in LUAD are not synthetic lethal in contrast to *KRAS* with co-occurring *EGFR* mutations. To explain the discrepancy in synthetic lethality compared to other studies, a functional head-to-head comparison of the two oncogenes located immediately vertically downstream of each other in the MAPK pathway would be necessary.

A comparable approach to our study was used by Ortiz-Cuaran et al., who found a *KRAS*^{G12S} mutation in a patient as a mechanism of resistance to osimertinib therapy[57]. In subsequent functional *in vitro* experiments, KRAS^{G12S}-mediated resistance was confirmed by sustained p-Erk signalling under EGFR-TKI therapy. The resistance could be overcome by the combined use of osimertinib with the MEK inhibitors trametinib or selumetinib and showed clear synergies. It is noteworthy that the cell lines exhibiting co-mutation of *EGFR* and *KRAS* demonstrated diminished cell viability initially; however, this was superseded following 10 passages of antibiotic selection[57].

The study by Ortiz-Cuaran et al. and the current study demonstrated that the combination of EGFR and MEK inhibitors effectively suppressed ERK activity and restored treatment

response, emphasising the importance of targeting both the primary driver and downstream signalling pathways.

4.3 Integration into the current study context

Recent developments in clinical oncology further support the concept of combination therapies. The MARIPOSA trial, a phase 3 study, investigated amivantamab, a bispecific EGFR- and MET-targeting antibody, combined with lazertinib, a third-generation EGFR-TKI, as first-line therapy for EGFR-mutant NSCLC. The combination resulted in a significant improvement in progression-free survival compared to osimertinib monotherapy (23.7 months vs. 16.6 months)[58]. The FLAURA2 trial, a phase 3 study, investigated osimertinib plus chemotherapy with pemetrexed and a platinum-based agent (cisplatin or carboplatin) against osimertinib monotherapy as first-line therapy in advanced EGFR-mutant NSCLC. The combination of osimertinib plus chemotherapy resulted in a significant improvement in progression-free survival compared to osimertinib monotherapy (25.5 months vs. 16.7 months) but patients also reported more and stronger adverse events[59]. Although the exact molecular mechanism of this combined therapy is unknown, it has been suggested that the non-selective effect of chemotherapy supports the selective effect of the EGFR-TKI to overcome intratumour heterogeneity[59]. Both studies underline the clinical potential of upfront combination strategies.

Beyond *EGFR*-mutated NSCLC, the concept of simultaneous inhibition of multiple targets from the MAPK pathway has been explored in other malignancies. In metastatic $BRAF^{V600E}$ mutated colorectal cancer, the combination of BRAF, EGFR, and MEK inhibitors led to improved MAPK pathway suppression and clinical benefit compared to dual inhibition strategies, highlighting the importance of targeting multiple nodes in adaptive signalling pathways. Similarly, in melanoma, combining BRAF inhibitors with MEK inhibitors proved to be more effective than single treatment, leading to this combination therapy becoming the new standard of care[60,61]
These collective findings across different tumour entities emphasize that simultaneous targeting of EGFR and the MAPK pathway is a broadly relevant therapeutic concept. The mechanistic rationale and the preclinical and clinical data derived from various settings strengthen the translational significance of the observations made in the present work.

4.4 Outlook on future research questions

An important question for future research is whether the resistance mechanisms observed after osimertinib monotherapy will remain relevant under possible new first-line combination regimens such as amivantamab plus lazertinib. It is conceivable that selective pressures may shift, leading to different patterns of resistance evolution. Therefore, continuous molecular monitoring using liquid biopsies and advanced imaging modalities will be crucial.

Moreover, proactive combination strategies, potentially including inhibitors of EGFR, MAPK and additional pathways, may become an effective approach to further delay the emergence of resistance. To refine therapeutic approaches, it will be essential to deepen the mechanistic understanding of how different co-mutations affect MAPK signalling dynamics, in particular contrasting the effects of KRAS and BRAF in the context of another mutation in the MAPK-pathway like *EGFR*.

4.5 Conclusion

The present study set out to investigate the role of both co-occurring and acquired *BRAF* mutations in patients with *EGFR* mutations. To validate the clinical data, a system with co-mutated $EGFR^{del19}$ and $BRAF^{V600E}$ was recreated *in vitro*, and a therapeutic option with combined EGFR and MEK inhibition was identified that was also effective in the *in vivo* xenograft model. In conclusion, this work provides further insights into the adaptive mechanisms of resistance in EGFR-mutant lung adenocarcinoma by demonstrating that $BRAF^{V600E}$-mediated MAPK reactivation drives therapeutic escape. Our clinical and functional data show that *EGFR/BRAF* co-mutation is not as synthetic lethal as many studies have suggested and that further experiments are needed to understand ERK-mediated synthetic lethality in the MAPK pathway, especially in comparison to KRAS. Furthermore, the data presented here fit within the broader evolution of treatment strategies towards upfront combination therapies, as exemplified by the MARIPOSA study and analogous strategies in other tumour entities. By contributing mechanistic and translational knowledge, this work advances the understanding of oncogene-driven resistance and lays a foundation for the development of future therapeutic strategies in EGFR-mutated NSCLC.

5. List of references

1 Unni AM, Lockwood WW, Zejnullahu K, Lee-Lin S-Q, Varmus H. Evidence that synthetic lethality underlies the mutual exclusivity of oncogenic KRAS and EGFR mutations in lung adenocarcinoma. *eLife* 2015; **4**: e06907.

2 Unni AM, Harbourne B, Oh MH, *et al.* Hyperactivation of ERK by multiple mechanisms is toxic to RTK-RAS mutation-driven lung adenocarcinoma cells. *eLife* 2018; **7**: e33718.

3 Timofeev O, Giron P, Lawo S, Pichler M, Noeparast M. ERK pathway agonism for cancer therapy: evidence, insights, and a target discovery framework. *Npj Precis Oncol* 2024; **8**: 70.

4 Bray F, Laversanne M, Sung H, *et al.* Global cancer statistics 2022: GLOBOCAN estimates of incidence and mortality worldwide for 36 cancers in 185 countries. *CA Cancer J Clin* 2024; **74**: 229–63.

5 Gridelli C, Rossi A, Carbone DP, *et al.* Non-small-cell lung cancer. *Nat Rev Dis Primer* 2015; **1**: 15009.

6 Schabath MB, Cote ML. Cancer Progress and Priorities: Lung Cancer. *Cancer Epidemiol Biomark Prev Publ Am Assoc Cancer Res Cosponsored Am Soc Prev Oncol* 2019; **28**: 1563–79.

7 Cargnello M, Roux PP. Activation and Function of the MAPKs and Their Substrates, the MAPK-Activated Protein Kinases. *Microbiol Mol Biol Rev MMBR* 2011; **75**: 50–83.

8 The Cancer Genome Atlas Research Network. Comprehensive molecular profiling of lung adenocarcinoma. *Nature* 2014; **511**: 543–50.

9 Yuan J, Dong X, Yap J, Hu J. The MAPK and AMPK signalings: interplay and implication in targeted cancer therapy. *J Hematol OncolJ Hematol Oncol* 2020; **13**: 113.

10 Guo Y-J, Pan W-W, Liu S-B, Shen Z-F, Xu Y, Hu L-L. ERK/MAPK signalling pathway and tumorigenesis. *Exp Ther Med* 2020; **19**: 1997–2007.

11 Santarpia L, Lippman SL, El-Naggar AK. Targeting the Mitogen-Activated Protein Kinase RAS-RAF Signaling Pathway in Cancer Therapy. *Expert Opin Ther Targets* 2012; **16**: 103–19.

12 Ullah R, Yin Q, Snell AH, Wan L. RAF-MEK-ERK pathway in cancer evolution and treatment. *Semin Cancer Biol* 2022; **85**: 123–54.

13 Zhang H, Berezov A, Wang Q, *et al.* ErbB receptors: from oncogenes to targeted cancer therapies. *J Clin Invest* 2007; **117**: 2051–8.

14 Nahar R, Zhai W, Zhang T, *et al.* Elucidating the genomic architecture of Asian EGFR-mutant lung adenocarcinoma through multi-region exome sequencing. *Nat Commun* 2018; **9**: 216.

15 Sharma SV, Bell DW, Settleman J, Haber DA. Epidermal growth factor receptor mutations in lung cancer. *Nat Rev Cancer* 2007; **7**: 169–81.

16 Rosell R, Cardona AF, Arrieta O, *et al.* Coregulation of pathways in lung cancer patients with EGFR mutation: therapeutic opportunities. *Br J Cancer* 2021; **125**: 1602–11.

17 O'Leary C, Gasper H, Sahin KB, *et al.* Epidermal Growth Factor Receptor (EGFR)-Mutated Non-Small-Cell Lung Cancer (NSCLC). *Pharmaceuticals* 2020; **13**: 273.

18 Stites EC. The Abundance of KRAS and RAS Gene Mutations in Cancer. In: Stephen AG, Esposito D, eds. KRAS: Methods and Protocols. New York, NY: Springer US, 2024: 13–22.

19 Prior IA, Hood FE, Hartley JL. The frequency of Ras mutations in cancer. *Cancer Res* 2020; **80**: 2969–74.

20 Sanchez-Vega F, Mina M, Armenia J, *et al.* Oncogenic Signaling Pathways in The Cancer Genome Atlas. *Cell* 2018; **173**: 321-337.e10.

21 Garnett MJ, Rana S, Paterson H, Barford D, Marais R. Wild-Type and Mutant B-RAF Activate C-RAF through Distinct Mechanisms Involving Heterodimerization. *Mol Cell* 2005; **20**: 963–9.

22 Davies H, Bignell GR, Cox C, *et al.* Mutations of the BRAF gene in human cancer. *Nature* 2002; **417**: 949–54.

23 Holderfield M, Deuker MM, McCormick F, McMahon M. Targeting RAF kinases for cancer therapy: BRAF mutated melanoma and beyond. *Nat Rev Cancer* 2014; **14**: 455–67.

24 Yao Z, Yaeger R, Rodrik-Outmezguine VS, *et al.* Tumours with class 3 BRAF mutants are sensitive to the inhibition of activated RAS. *Nature* 2017; **548**: 234–8.

25 Owsley J, Stein MK, Porter J, *et al.* Prevalence of class I–III BRAF mutations among 114,662 cancer patients in a large genomic database. *Exp Biol Med* 2021; **246**: 31.

26 Heidorn SJ, Milagre C, Whittaker S, *et al.* Kinase-Dead BRAF and Oncogenic RAS Cooperate to Drive Tumor Progression through CRAF. *Cell* 2010; **140**: 209–21.

27 Weinstein IB. Cancer. Addiction to oncogenes--the Achilles heal of cancer. *Science* 2002; **297**: 63–4.
28 Weinstein IB, Joe AK. Mechanisms of Disease: oncogene addiction—a rationale for molecular targeting in cancer therapy. *Nat Clin Pract Oncol* 2006; **3**: 448–57.
29 Sharma SV, Settleman J. Oncogene addiction: setting the stage for molecularly targeted cancer therapy. *Genes Dev* 2007; **21**: 3214–31.
30 Lynch TJ, Bell DW, Sordella R, *et al.* Activating Mutations in the Epidermal Growth Factor Receptor Underlying Responsiveness of Non–Small-Cell Lung Cancer to Gefitinib. *N Engl J Med* 2004; **350**: 2129–39.
31 Planchard D, Smit EF, Groen HJM, *et al.* Dabrafenib plus trametinib in patients with previously untreated BRAFV600E-mutant metastatic non-small-cell lung cancer: an open-label, phase 2 trial. *Lancet Oncol* 2017; **18**: 1307–16.
32 Mok TS, Wu Y-L, Thongprasert S, *et al.* Gefitinib or Carboplatin–Paclitaxel in Pulmonary Adenocarcinoma. *N Engl J Med* 2009; **361**: 947–57.
33 Sharma SV, Fischbach MA, Haber DA, Settleman J. 'Oncogenic shock': explaining oncogene addiction through differential signal attenuation. *Clin Cancer Res Off J Am Assoc Cancer Res* 2006; **12**: 4392s–5s.
34 Sharma SV, Settleman J. Exploiting the balance between life and death: Targeted cancer therapy and "oncogenic shock". *Biochem Pharmacol* 2010; **80**: 666–73.
35 Luo J, Solimini NL, Elledge SJ. Principles of Cancer Therapy: Oncogene and Non-oncogene Addiction. *Cell* 2009; **136**: 823–37.
36 Freije JMP, Fraile JM, López-Otín C. Protease Addiction and Synthetic Lethality in Cancer. *Front Oncol* 2011; **1**: 25.
37 Nagel R, Semenova EA, Berns A. Drugging the addict: non-oncogene addiction as a target for cancer therapy. *EMBO Rep* 2016; **17**: 1516–31.
38 Petti C, Molla A, Vegetti C, Ferrone S, Anichini A, Sensi M. Coexpression of NRASQ61R and BRAFV600E in human melanoma cells activates senescence and increases susceptibility to cell-mediated cytotoxicity. *Cancer Res* 2006; **66**: 6503–11.
39 Howlader N, Forjaz G, Mooradian MJ, *et al.* The Effect of Advances in Lung-Cancer Treatment on Population Mortality. *N Engl J Med* 2020; **383**: 640–9.
40 Solassol I, Pinguet F, Quantin X. FDA- and EMA-Approved Tyrosine Kinase Inhibitors in Advanced EGFR-Mutated Non-Small Cell Lung Cancer: Safety, Tolerability, Plasma Concentration Monitoring, and Management. *Biomolecules* 2019; **9**: 668.
41 Tulpule A, Bivona TG. Acquired Resistance in Lung Cancer. *Annu Rev Cancer Biol* 2020; **4**: 279–97.
42 Yu HA, Arcila ME, Rekhtman N, *et al.* Analysis of Tumor Specimens at the Time of Acquired Resistance to EGFR TKI therapy in 155 patients with EGFR mutant Lung Cancers. *Clin Cancer Res Off J Am Assoc Cancer Res* 2013; **19**: 2240–7.
43 Pao W, Miller VA, Politi KA, *et al.* Acquired Resistance of Lung Adenocarcinomas to Gefitinib or Erlotinib Is Associated with a Second Mutation in the EGFR Kinase Domain. *PLoS Med* 2005; **2**: e73.
44 Sos ML, Rode HB, Heynck S, *et al.* Chemogenomic profiling provides insights into the limited activity of irreversible EGFR Inhibitors in tumor cells expressing the T790M EGFR resistance mutation. *Cancer Res* 2010; **70**: 868–74.
45 Katakami N, Atagi S, Goto K, *et al.* LUX-Lung 4: a phase II trial of afatinib in patients with advanced non-small-cell lung cancer who progressed during prior treatment with erlotinib, gefitinib, or both. *J Clin Oncol Off J Am Soc Clin Oncol* 2013; **31**: 3335–41.
46 Kobayashi S, Boggon TJ, Dayaram T, *et al.* EGFR Mutation and Resistance of Non–Small-Cell Lung Cancer to Gefitinib. *N Engl J Med* 2005; **352**: 786–92.
47 Chhouri H, Alexandre D, Grumolato L. Mechanisms of Acquired Resistance and Tolerance to EGFR Targeted Therapy in Non-Small Cell Lung Cancer. *Cancers* 2023; **15**: 504.
48 Jänne PA, Yang JC-H, Kim D-W, *et al.* AZD9291 in EGFR inhibitor-resistant non-small-cell lung cancer. *N Engl J Med* 2015; **372**: 1689–99.
49 Mok TS, Wu Y-L, Ahn M-J, *et al.* Osimertinib or Platinum-Pemetrexed in EGFR T790M-Positive Lung Cancer. *N Engl J Med* 2017; **376**: 629–40.
50 Soria J-C, Ohe Y, Vansteenkiste J, *et al.* Osimertinib in Untreated EGFR-Mutated Advanced Non-

Small-Cell Lung Cancer. *N Engl J Med* 2018; **378**: 113–25.
51 Ramalingam SS, Vansteenkiste J, Planchard D, *et al.* Overall Survival with Osimertinib in Untreated, EGFR-Mutated Advanced NSCLC. *N Engl J Med* 2020; **382**: 41–50.
52 Leonetti A, Sharma S, Minari R, Perego P, Giovannetti E, Tiseo M. Resistance mechanisms to osimertinib in EGFR-mutated non-small cell lung cancer. *Br J Cancer* 2019; **121**: 725–37.
53 Ramalingam SS, Cheng Y, Zhou C, *et al.* Mechanisms of acquired resistance to first-line osimertinib: Preliminary data from the phase III FLAURA study. *Ann Oncol* 2018; **29**: viii740.
54 Schaufler D, Ast DF, Tumbrink HL, *et al.* Clonal dynamics of BRAF-driven drug resistance in EGFR-mutant lung cancer. *Npj Precis Oncol* 2021; **5**: 102.
55 Beijersbergen RL, Wessels LFA, Bernards R. Synthetic Lethality in Cancer Therapeutics. *Annu Rev Cancer Biol* 2017; **1**: 141–61.
56 Huang L, Guo Z, Wang F, Fu L. KRAS mutation: from undruggable to druggable in cancer. *Signal Transduct Target Ther* 2021; **6**: 386.
57 Ortiz-Cuaran S, Scheffler M, Plenker D, *et al.* Heterogeneous Mechanisms of Primary and Acquired Resistance to Third-Generation EGFR Inhibitors. *Clin Cancer Res* 2016; **22**: 4837–47.
58 Cho BC, Lu S, Felip E, *et al.* Amivantamab plus Lazertinib in Previously Untreated EGFR-Mutated Advanced NSCLC. *N Engl J Med* 2024; **391**: 1486–98.
59 Planchard D, Jänne PA, Cheng Y, *et al.* Osimertinib with or without Chemotherapy in EGFR-Mutated Advanced NSCLC. *N Engl J Med* 2023; **389**: 1935–48.
60 Long GV, Stroyakovskiy D, Gogas H, *et al.* Combined BRAF and MEK Inhibition versus BRAF Inhibition Alone in Melanoma. N. Engl. J. Med. 2014; published online Nov 13. DOI:10.1056/NEJMoa1406037.
61 Schulz A, Raetz J, Karitzky PC, *et al.* Head-to-Head Comparison of BRAF/MEK Inhibitor Combinations Proposes Superiority of Encorafenib Plus Trametinib in Melanoma. *Cancers* 2022; **14**: 4930.

6. Appendix

6.1 Supplementary material paper

Supplementary Material

Supplementary Table 1 (A-D) ^{18}FDG-PET/CT assessment for monitoring of metabolic response during different lines of treatment of two patients with *EGFR*/*BRAF*-mutant lung adenocarcinoma. Table summarizes the standard uptake values (SUV). **(A)** P01, lesion 1; **(B)** P01, lesion 2; **(C)** P04, lesion 1; **(D)** P04, lesion 2. D+T, dabrafenib+trametinib; O+D(+T), osimertinib+dabrafenib(+trametinib);O(+CTX)+B,osimertinib(+chemotherapy)+bevacizumab; A+C, afatinib+crizotinib; O+TACE, osimertinib+transarterial chemoembolization; FU, Follow-up; PD, progressive disease.

A

Treatment	^{18}FDG-PET/CT assessments		Left upper lung lobe (initially hottest lesion) SUVmax
D+T	BASELINE	28.11.2018	11,64
D+T	2 WeFU	19.12.2018	9,49
D+T	6 WeFU	16.01.2019	10,64
D+T	10 WeFU	18.02.2019	11,89
O+D	2 WeFU	13.03.2019	14,46
A+C	2 WeFU	09.04.2019	8,12
A+C	6 WeFU	08.05.2019	10,91
O+D+T	3 WeFU	26.06.2019	9,83
O+D+T	7 WeFU	29.07.2019	11,89
O+D+T	12 WeFU	12.09.2019	7,74
O+D+T	20 WeFU	12.11.2019	8,07
O+D+T	32 WeFU	13.02.2020 (only CT)	Morphological PD
O+D+T	9 MoFU	20.03.2019	7,13
O+Beva (2x)	6 WeFU	06.05.2020	11,96
A+C	3 WeFU	09.06.2020	8,83
A+C	12 WeFU	18.08.2020	8,68 new PET positive retroperitoneal metastases
O+D+T	not done	not done	not done

B

Treatment	^{18}FDG-PET/CT assessments		Left lower lung lobe SUVmax
D+T	BASELINE	28.11.2018	10,36
D+T	2 WeFU	19.12.2018	6,29
D+T	6 WeFU	16.01.2019	8,20
D+T	10 WeFU	18.02.2019	8,24
O+D	2 WeFU	13.03.2019	11,01
A+C	2 WeFU	09.04.2019	6,24
A+C	6 WeFU	08.05.2019	10,84
O+D+T	3 WeFU	26.06.2019	9,39
O+D+T	7 WeFU	29.07.2019	7,74
O+D+T	12 WeFU	12.09.2019	5,24
O+D+T	20 WeFU	12.11.2019	6,95
O+D+T	32 WeFU	13.02.2020 (only CT)	Morphological PD
O+D+T	9 MoFU	20.03.2019	6,44
O+Beva (2x)	6 WeFU	06.05.2020	10,01
A+C	3 WeFU	09.06.2020	7,52
A+C	12 WeFU	18.08.2020	5,53 new PET positive retroperitoneal metastases
O+D+T	not done	not done	not done

C

Treatment	^{18}FDG-PET/CT assessments		Right upper lung lobe (hottest lesion) SUVmax
D+T	BASELINE	13.11.2018	8,41
D+T	2 WeFU	21.12.2018	12,25
D+T	6 WeFU	08.01.2019	10,99
O+D	2 WeFU	28.01.2019	9,05
O+D	6 WeFU	27.02.2019	10,89
O+D	12 WeFU	10.04.2019	10,56
O+D+T	2 WeFU	20.05.2019	5,91
O+D+T	6 WeFU	21.06.2019	10,46
O+CTX+B (2x)	4 WeFU	22.08.2019	6.37
O+TACE	not done	not done	not done

D

Treatment	^{18}FDG-PET/CT assessments		Right liver lobe metastasis SUVmax
D+T	BASELINE	13.11.2018	5,73
D+T	2 WeFU	21.12.2018	6,01
D+T	6 WeFU	08.01.2019	5,91
O+D	2 WeFU	28.01.2019	3,47
O+D	6 WeFU	27.02.2019	4,30
O+D	12 WeFU	10.04.2019	4,17
O+D+T	2 WeFU	20.05.2019	7,13
O+D+T	6 WeFU	21.06.2019	7,58
O+CTX+B (2x)	4 WeFU	22.08.2019	6,26
O+TACE	not done	not done	not done

Supplementary Table 2 (A,B) Treatment strategy, dose regimen and treatment-related adverse events according to Common Terminology Criteria for Adverse Events (CTCAE) Version 5.0. AEs of higher grade were mostly mixed disease- and treatment-related effects. **(A)** P01; **(B)** P04. D+T, dabrafenib+trametinib; O+D(+T), osimertinib+dabrafenib (+trametinib);O(+CTX)+B, osimertinib(+chemotherapy)+bevacizumab; A+C, afatinib+ crizotinib; O+TACE, osimertinib+transarterial chemo- embolization; TTD, time-to-treatment discontinuation; AE, adverse event.

A

Treatment	Start-Stop	Dose regimen	TTD (days)	AEs	Comments
D+T	06.12.2018-18.02.2019	dabrafenib 150mg 1-0-1 trametinib 2mg 0-0-1	74	Hyponatremia Grade II-III; GGT/AP increased Grade I-II; Fever Grade II-III; Nausea Grade I; Lipase/Amylase increased Grade I-II; Fatigue Grade I; Anorexia Grade I; Panniculitis Grade I-II; Anemia Grade I;	
O+D	22.02.2019-21.03.2019	osimertinib 80mg 0-0-1 dabrafenib 150mg 1-0-1	27	Lipase/Aamylase increased Grade II-III; GGT/AP increased Grad I; Anemia Grade I;	Intermittent interruption of O+D due to increase in amylase and lipase (no signs of pancreatitis);
A+C	24.03.2019-28.05.2019	afatinib 40mg 1-0-0 crizotinib 200mg 1-0-1	65	Rash maculo-papular Grade I-II; Diarrhea Grade I; Lipase/ Amylase increased Grade I-II; Nausea Grade I; Edema Grade I; Dry eyes Grade I; Anorexia Grade I; Paronychia Grade I-II; Anemia Grade I;	Intermittent interruption and/or dose reduction of A+C;
O+D+T	05.06.2019-19.03.2020	osimertinib 80mg 0-0-1 dabrafenib 150mg 1-0-1 trametinib 2mg 0-0-1	288	Lipase/Amylase increased Grade II-III; GGT/AP increased Grade I; Hyponatremia Grade II-III; Diarrhea Grade I; Fever Grade I-II; Nausea Grade I; Fatigue Grade I; Anorexia Grade I; Ascites Grade II; Anemia Grade II-III; Edema Grade I;	Intermittent interruption of O+D+T due to increase in amylase and lipase (no symptoms of pancreatitis); Ascites was associated to peritoneal carcinosis and cirrhosis (paracentesis); Tolvaptan treatment was administered for hypo-natremia;
O+B	20.03.2020-12.05.2020	osimertinib 80mg 1-0-0 bevacizumab 15mg/kg Q3W (2x)	53	Ascites Grade II; Fatigue Grade II; Anorexia Grade II; Anemia Grade II; Edema Grade I-II; GGT increased Grade I;	Ascites/Edema/Fatigue/Anorexia were associated with tumor progression, pre-existing cirrhosis and hypo-albuminemia;
A+C	17.05.2020-30.08.2020	afatinib 30mg 1-0-0 crizotinib 250mg 1-0-1, later afatinib was reduced to 20 mg 1-0-0 and crizotinib to 200mg 1-0-1	105	Ascites Grade II-III; Fatigue Grade II; Anorexia Grade II; Anemia Grade II; Edema Grade I-II; Rash Grade I-II; GGT/AP increased Grade I-II; Diarrhea Grade I-II; Nausea Grade II;	Intermittent interruption and/or dose reduction of afatinib and crizotinib due to rash, edema, diarrhea or nausea;
O+D+T	02.09.2020-ongoing	osimertinib 80mg 0-0-1 dabrafenib 150mg 1-0-1 trametinib 2mg 0-0-1	na	Ascites Grade II-III; Fatigue Grade II; Anorexia Grade II; Anemia Grade II; Edema Grade I-II; GGT/AP increased Grade I-II; Diarrhea Grade I-II; Nausea Grade II;	

B

Treatment	Start-Stop	Dose regimen	TTD (days)	AEs	Comments
D+T	06.12.2018-13.01.2019	dabrafenib 150mg 1-0-1 trametinib 2mg 0-0-1	38	Nausea Grade I; Vomiting Grad I; GGT/AP increased Grade I; Fatigue Grade I; Fever Grade I; Dry mouth Grade I; Myalgia Grade I-II;	Increase in AP/GGT were associated with liver metastases;
O+D	14.01.2019-17.04.2019	osimertinib 80mg 0-0-1 dabrafenib 150mg 1-0-1	93	Nausea Grade I; Fatigue Grade I; GOT/GPT increased Grade I; GGT/AP increased Grade II-III; Cough Grade I; Lipase increased Grade I; Myalgia Grade I-II; Anorexia Grade I;	Increase in GOT/GPT can be related to treatment; Increase in AP/GGT can be associated with liver metastases; Cough was possibly associated with respiratory infection and resolved within a few days;
O+D+T	18.04.2019-04.07.2019	osimertinib 80mg 0-0-1 dabrafenib 150mg 1-0-1 trametinib 2mg 0-0-1, from 30.04.2019 trametinib was reduced to 1mg 0-0-1	77	Myalgia Grade II; Anorexia Grade I; GGT/AP increased Grade II; Fatigue Grade I; Fever Grade I;	Dose of trametinib was reduced which improved myalgia and fatigue symptoms;
O+CTX+B	05.07.2019-18.09.2019	osimertinib 80mg 1-0-0 carboplatin AUC 6 and pemetrexed 500 mg/m^2 (2x cycles; 2nd cycle: AUC 4 and 250/m^2) bevacizumab 15 mg/kg Q3W (2x cycles)	75	Fatigue Grade II; Anorexia II-III; GGT/AP increased Grade II-III; Fatigue Grade I;	Second cycle of chemotherapy was dose reduced due to clinical deterioration of the patient.
O+TACE	19.09.2019-Nk.09.2019	osimertinib 80mg 1-0-0	na	Ascites Grade II-III; Fatigue Grade II; Anorexia Grade II; Anemia Grade II; Edema Grade I-II; GGT/AP increased Grade I-II; Diarrhea Grade I-II; Nausea Grade II;	

Supplementary Table 3 Used Primers

Sequence	Purpose
CTAAGCCTCCGCCTCCTC	pBabe seq f
GACTAATTGAGATGCATG	pBabe seq r
TCCGCTGTCAAACATGTGGT	seq PBABE V600E inside Braf-casette
TCGTGGTGATGGAGGATCAAC	BRAF qPCR f
TCATCACTCGAGTCCCGTCT	BRAF qPCR r
CAGGTGGTGTTGGGAAAAGC	NRAS qPCR f
TCAACACCCTGTCTGGTCTT	NRAS qPCR r

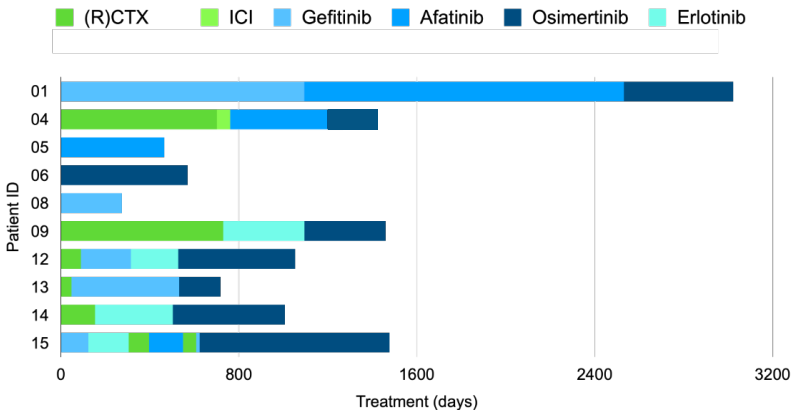

Supplementary Figure 1. Treatment history before the detection of acquired *BRAF* mutations in 10 patients evaluable for treatment history.

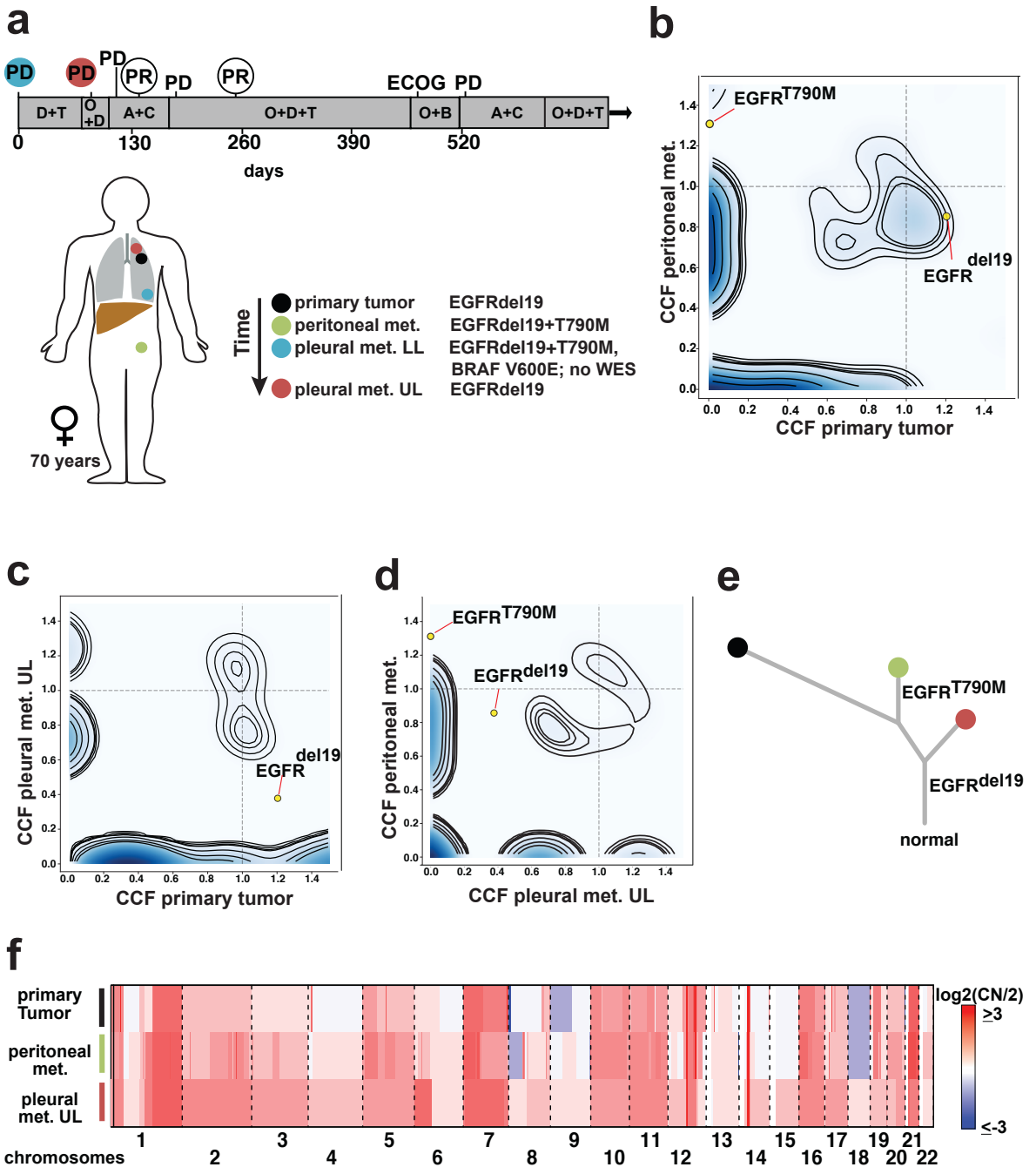

Supplementary Figure 2. (**a**) Overview of the biopsies and key molecular findings by targeted NGS for patient 01 and flow chart summarizing lines of therapy approaches over time after the acquisition of *BRAF*^{V600E} mutation following osimertinib. (**b-d**) Pairwise clustering of WES-derived mutations based on their CCFs between pairs of tumor biopsies. Large clusters of private mutations indicate a high degree of genetic dissimilarity between biopsies. Candidate mutations in *EGFR* are highlighted. (**e**) Visualization of genetic distances between normal tissue and longitudinal biopsies in a phylogenetic tree. Branching indicates that the metastases and the primary tumor derived from a shared common ancestor. (**f**) Profiles of purity and ploidy corrected copy number (CN) in the metastases. (red = CN gain, blue = CN loss). *EGFR*, epidermal growth factor receptor; *BRAF*, B-rapidly accelerated fibrosarcoma; WES, whole-exome sequencing; NGS, next-generation sequencing; PD, progressive disease; PR, partial response; D+T, dabrafenib+trametinib; O+D(+T), osimertinib+dabrafenib(+trametinib); A+C, afatinib+crizotinib; O+B, osimertinib+bevacizumab; ECOG, Eastern Cooperative Oncology Group; CCF, cancer cell fraction; LL, lower lobe; UL, upper lobe.

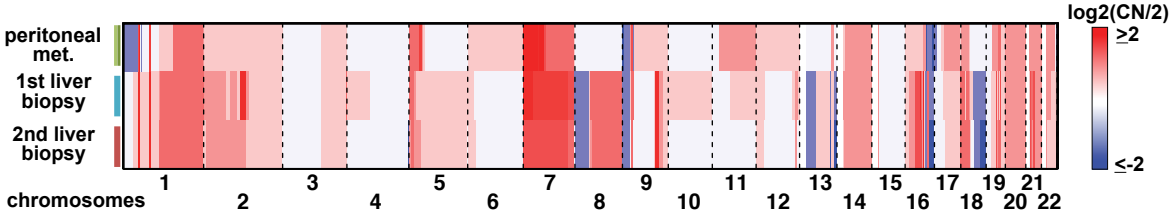

Supplementary Figure 3. Profiles of purity and ploidy corrected copy number (CN) in the metastases (red = CN gain, blue = CN loss) for patient P04.

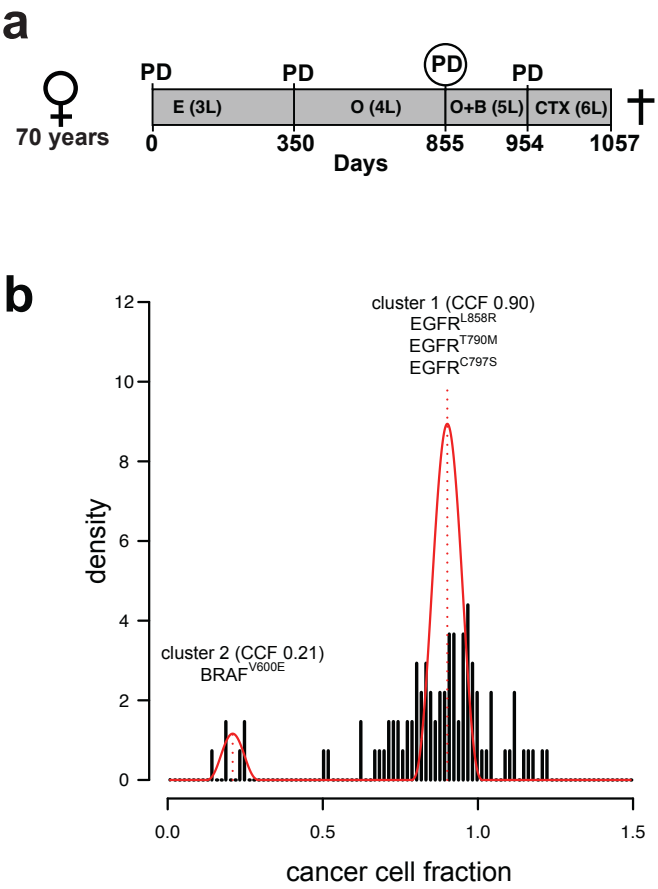

Supplementary Figure 4. (**a**) Overview of the treatment lines for patient P14 after erlotinib was started. Biopsy for WES obtained at the time of progression after osimertinib treatment was taken at day 855. (**b**) WES-based clonality analysis of the biopsy displayed two mutation clusters with corresponding cancer cell fractions (CCF). Relevant mutations are indicated above the corresponding clusters. *EGFR*, epidermal growth factor receptor; *BRAF*, B-rapidly accelerated fibrosarcoma; WES, whole-exome sequencing; PD, progressive disease; E, erlotinib; O, osimertinib; O+B, osimertinib+bevacizumab; CTX, chemotherapy. L, line of therapy.

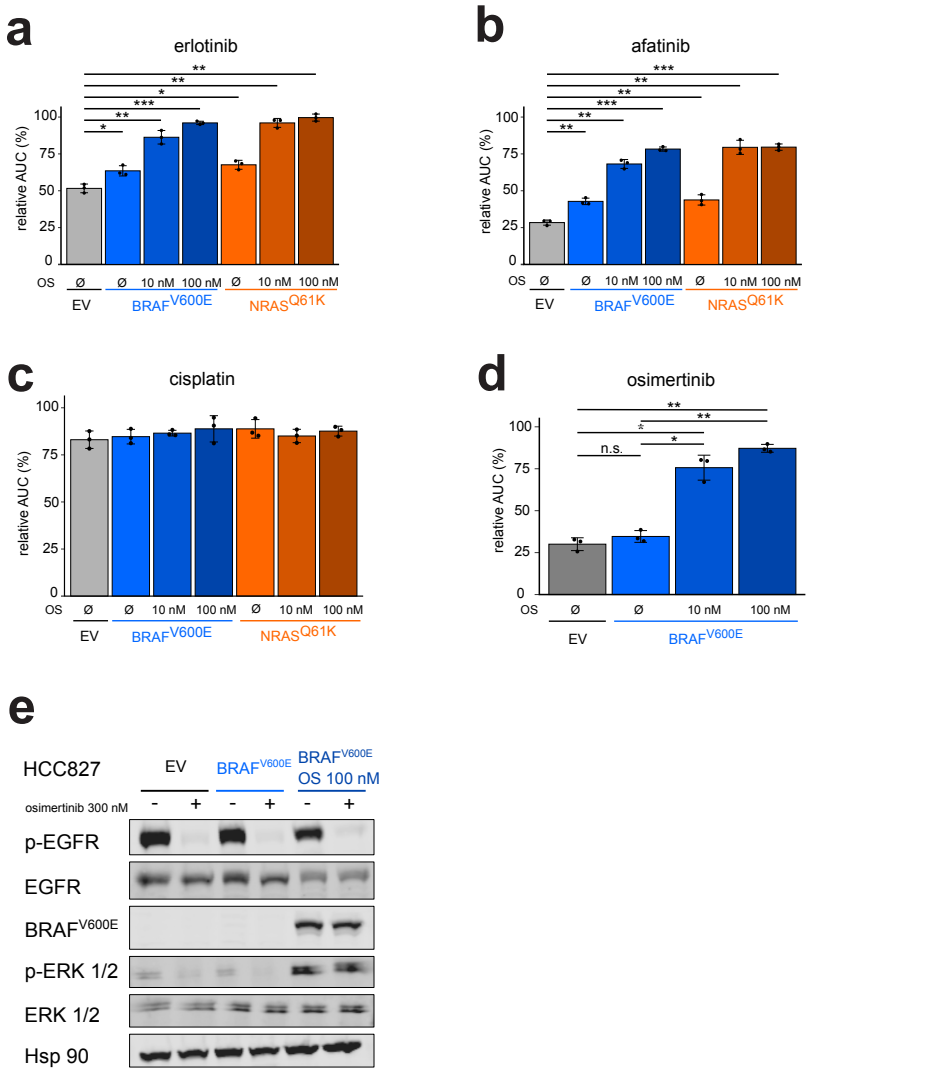

Supplementary Figure 5. (**a-c**) Viability assay of PC9 derived cell lines, treated for 72 hours with (**a**) erlotinib, (**b**) afatinib or (**c**) cisplatin. (**d**) Viability assay of HCC827 derived cell lines treated with osimertinib (72h) are shown. (**e**) Immunoblotting of HCC827 cells expressing the annotated constructs, treated with (+) or without (-) osimertinib (48h) and Hsp90 is used as loading control. The relative area under the curve (AUC) in % compared to a theoretical non-responding AUC. Error bars indicate mean ± SD. Two-tailed paired t-tests, ***p < 0.001, **p < 0.01, *p < 0.05.

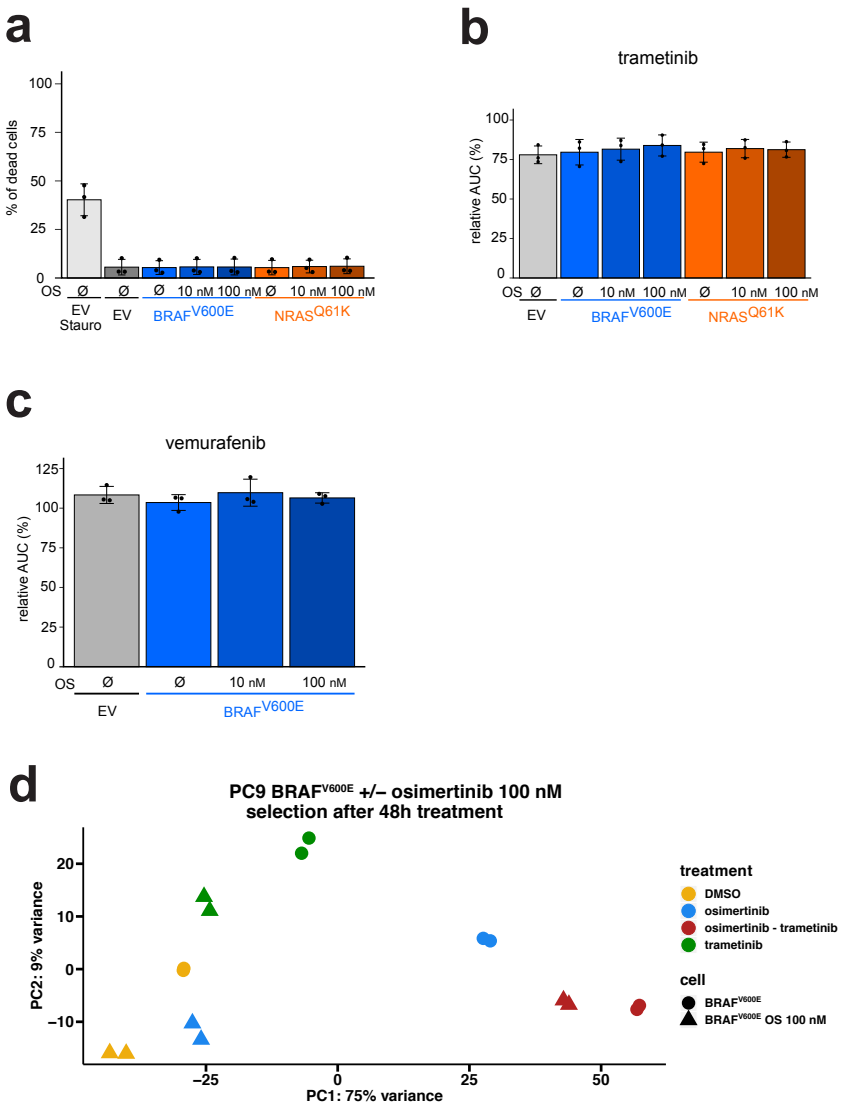

Supplementary Figure 6. (**a**) Percentage of dead cells measured by flow cytometry. Staurosporine control treated for 24 hours. (**b,c**) Viability assay of PC9 (EV) derived cell lines, treated for 72 hours with (**b**) trametinib or (**c**) vemurafenib. (**d**) Principal component analysis of 3'UTR-RNA-seq-samples in duplicates. The relative area under the curve (AUC) in % compared to a theoretical non-responding AUC. Error bars indicate mean ± SD. Two-tailed paired t-tests, *** $p < 0.001$, ** $p < 0.01$, * $p < 0.05$.

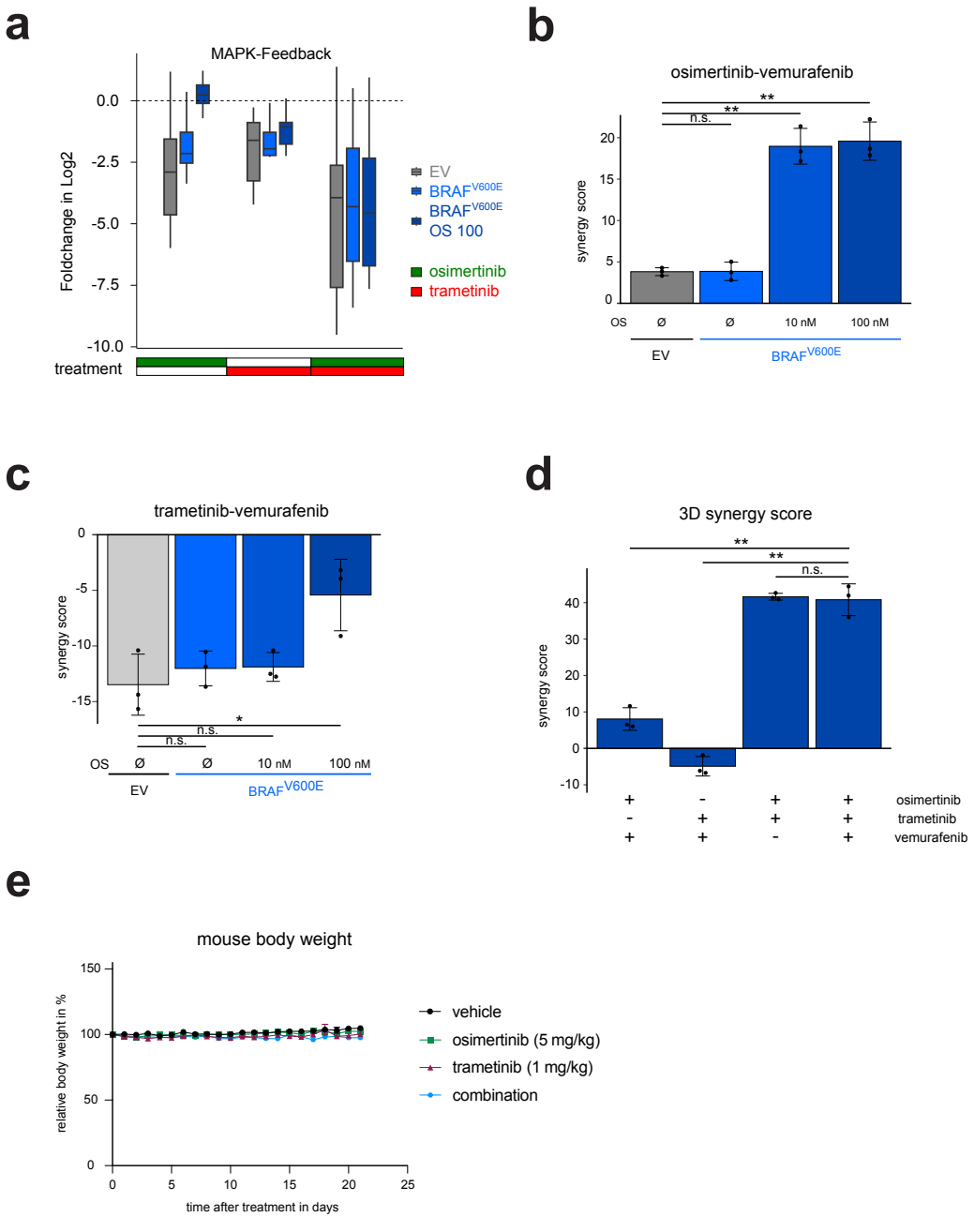

Supplementary Figure 7. (**a**) RNA-seq based log2 fold-changes of negative MAPK feedback genes (see methods) of PC9 derived cell lines after 48h treatment with indicated inhibitors compared to their respective DMSO controls. (**b**) Synergy screen of osimertinib and vemurafenib combination treatment in PC9 derived cell lines for 72 hours. (**c**) Synergy screen of trametinib and vemurafenib combination treatment in PC9 derived cell lines for 72 hours. (**d**) 3D Synergy screen of osimertinib, trametinib and vemurafenib combination treatment in PC9 pBABE BRAFV600E OS 100 cells for 72 hours. (**e**) Relative body weight of all mice in trial (see methods) in % compared to day 0. Error bars indicate mean ± SD. Two-tailed paired t-tests, *** $p < 0.001$, ** $p < 0.01$, * $p < 0.05$.

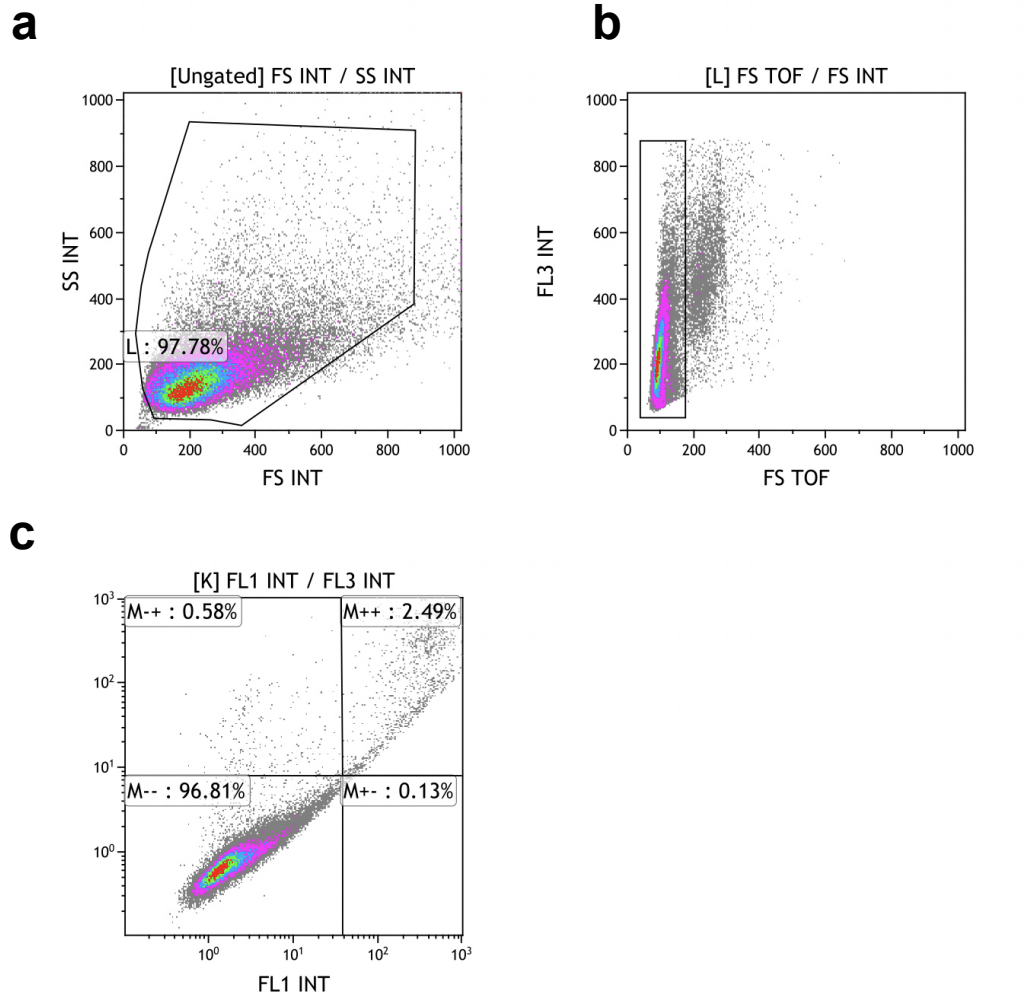

Supplementary Figure 8. Flow cytometry gating strategy. Apoptosis assay using flow cytometry after staining with annexin V-FITC/propidium iodide (PI). (**a**) Total cells were first gated on a forward scatter (FS)/side scatter (SS) for total counted events. (**b**) Cells were gated on a FS area versus FS width density plot to remove doublet cells. (**c**) Representative scatter plots of PI (y-axis) vs. annexin V (x-axis).

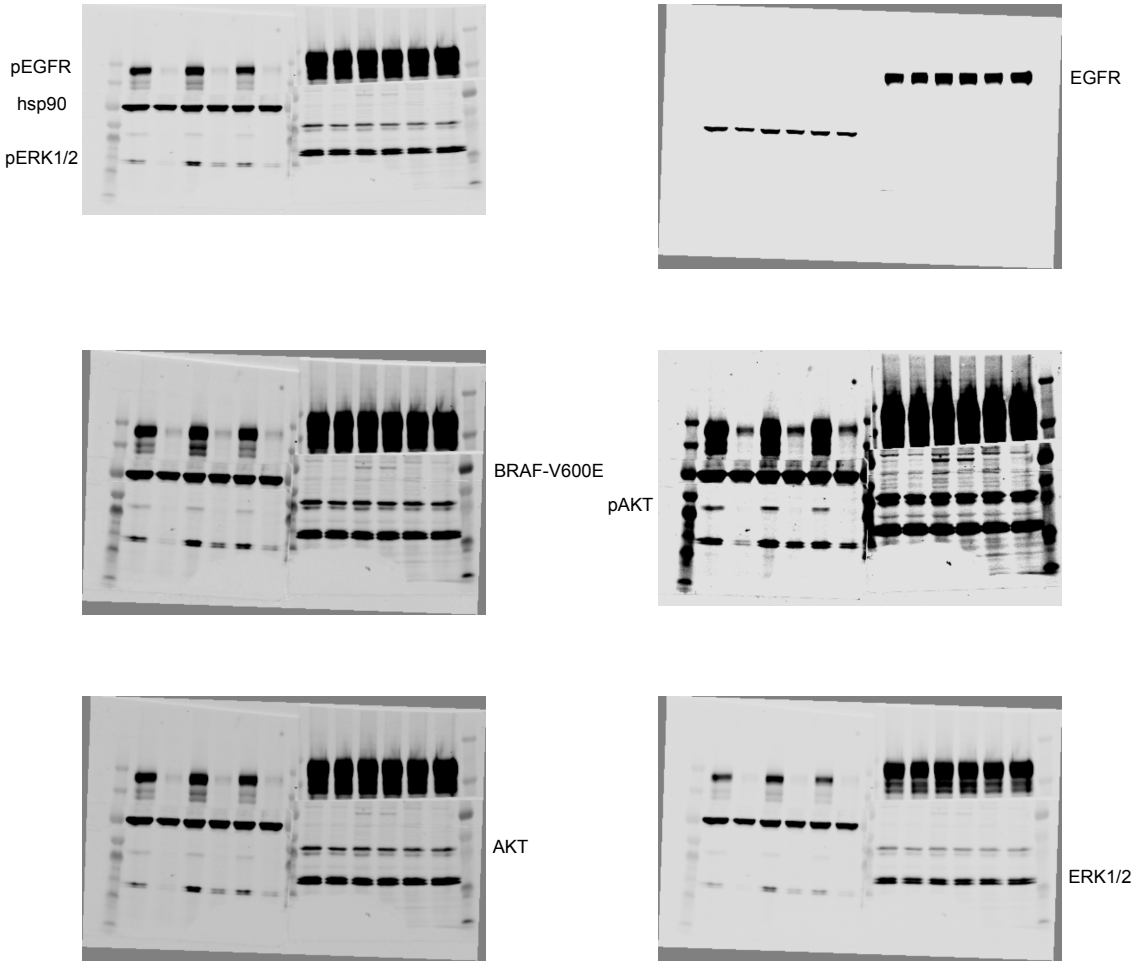

Supplementary Figure 9. Uncropped Blots of Figure 2a

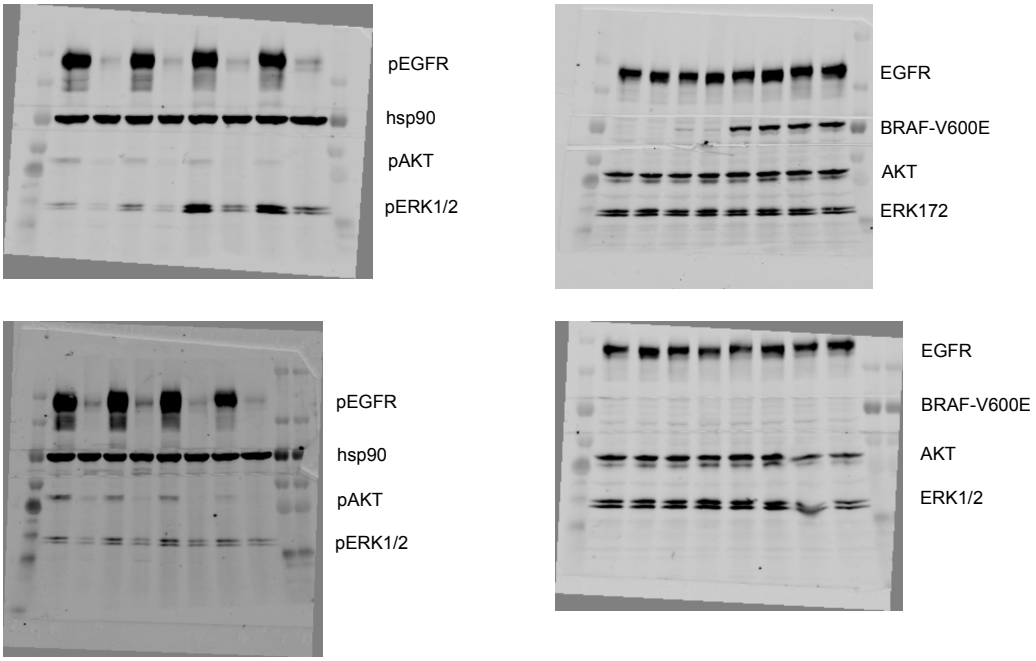

Supplementary Figure 10. Uncropped blots of Figure 2g

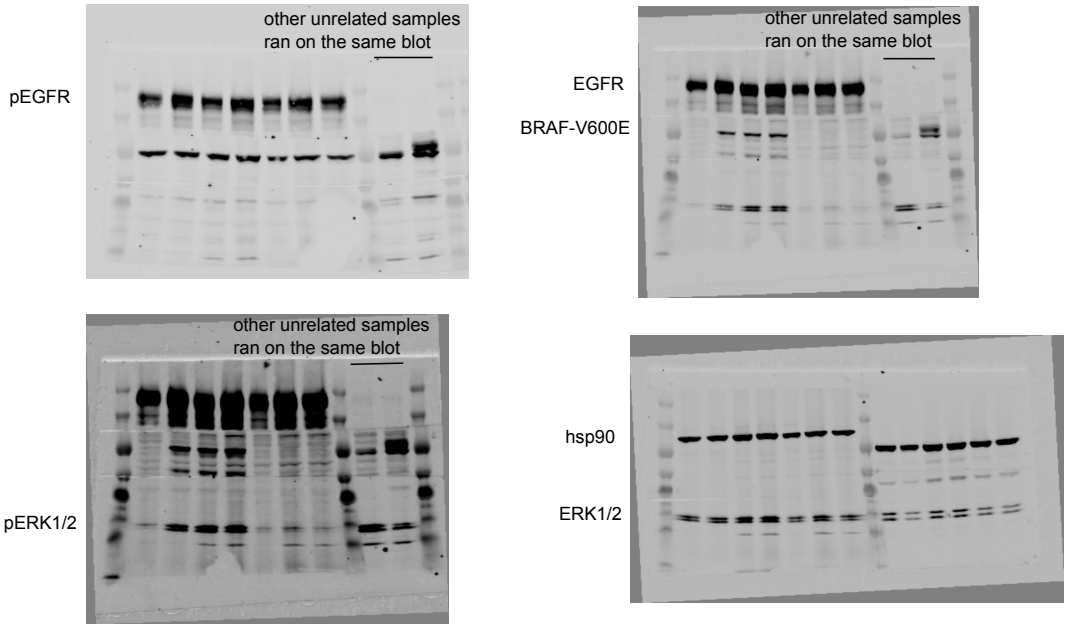

Supplementary Figure 11. Uncropped blots of Figure 3b

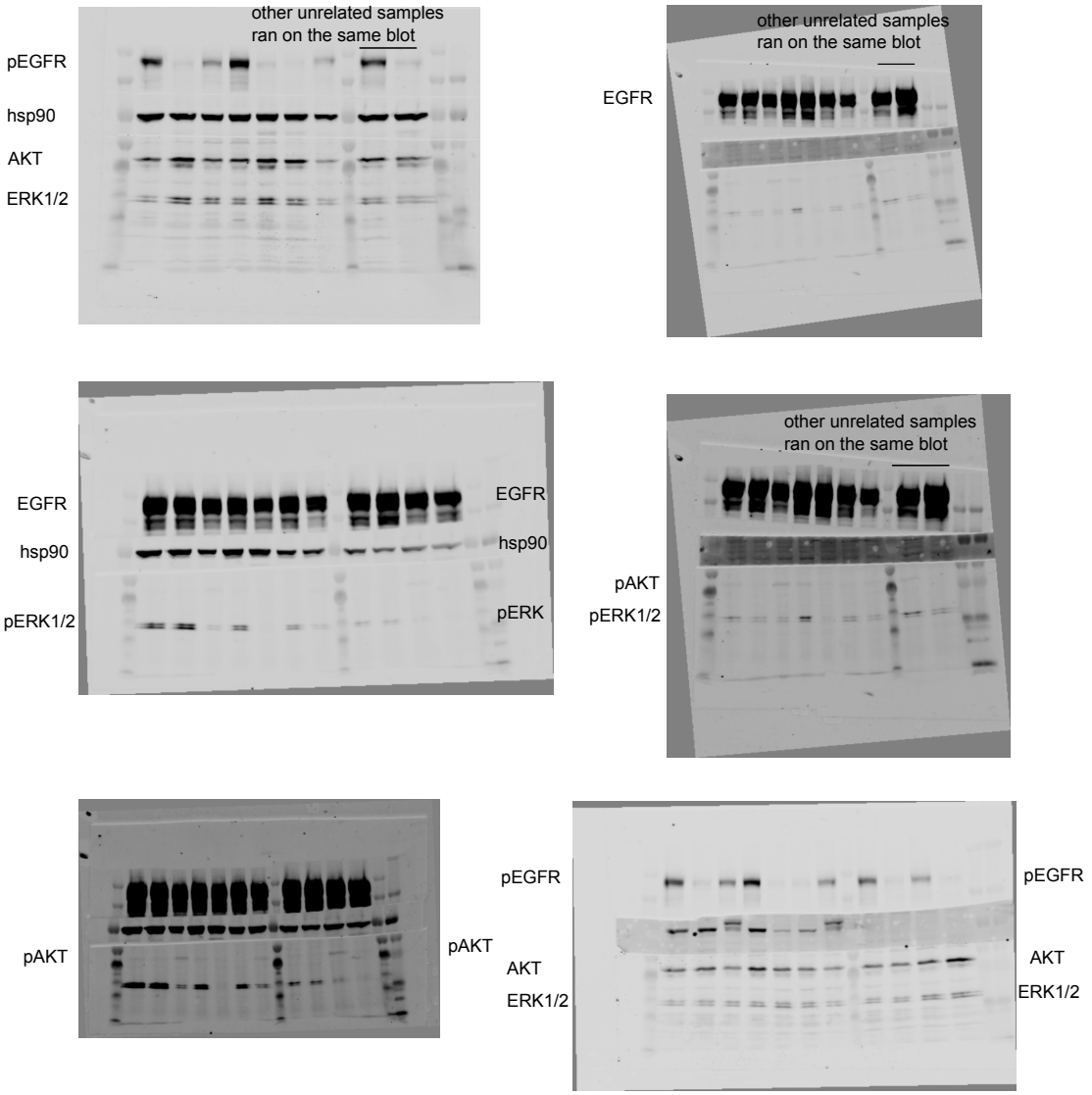

Supplementary Figure 12. Uncropped blots of Figure 3g

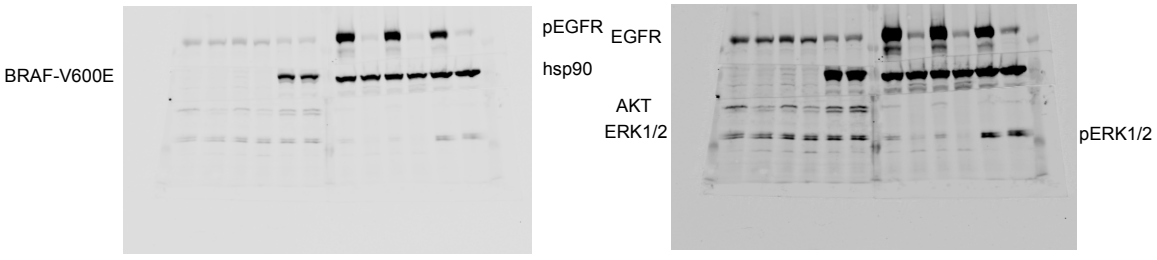

Supplementary Figure 13. Uncropped blots of Supplementary Figure 5e